THERMAL HISTORY OF

THE GRANULITIC IMPACTITE SUITE

ROCKS FROM THE LUNAR HIGHLANDS

*

A THESIS SUBMITTED TO THE GRADUATE DIVISION OF THE
UNIVERSITY OF HAWAII IN PARTIAL FULFILLMENT OF THE
REQUIREMENTS FOR THE DEGREE OF

MASTER OF SCIENCE

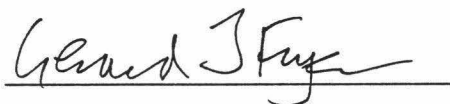IN

GEOLOGY

DECEMBER 1993

By

Janet A. Cushing

Thesis Committee:

G. Jeffrey Taylor, Chairperson
Gerard Fryer
Klaus Keil
John Sinton

We certify that we have read this thesis and that, in our opinion, it is satisfactory in scope and quality as a thesis for the degree of Master of Science in Geology.

THESIS COMMITTEE

_____
Chairperson

_____

_____

_____

ii

ACKNOWLEDGEMENTS

how to use the microprobe. Thanks also go to Noel Ludwig for interesting discussions on measuring grains and vugs, and launching rubber bands.

The cameraderie among the faculty and students in Planetary Geosciences has been wonderful, and hopefully they will stay as tight-knit a group when/if the POST building becomes occupied. I thank my officemates for putting up with me and my eccentricities. I thank the Boyz Club for pleasant Friday afternoons and providing an intriguing look into the male domain. Finally, I thank Dave Foss, Sara Finnemore, Sarah Sherman, Rachel Friedman, Tina Mueller, and others that I've forgotten to mention for making my stay in Hawaii a wonderful experience. Mahalo!

iv

TABLE OF CONTENTS

LIST OF TABLES

LIST OF TABLES (Continued)

LIST OF FIGURES

LIST OF ABBREVIATIONS

keV: kiloelectron volt

nA: nanoamps

μm: micrometer

mm: millimeter

cm: centimeter

m: meter

km: kilometer

kbar: kilobar

x (e.g., 63x): times

Yr: years

wt. %: weight percent

En: enstatite

Fs: ferrosillite

Wo: wollastanite

Di: diopside

Hd: hedenbergite

Aug: augite

Opx: orthopyroxene

Pig: pigeonite

°C: degrees Celsius

Elements

Al: Aluminum

Ca: Calcium

Cr: Chromium

Fe: Iron

Mg: Magnesium

Mn: Manganese

Na: Sodium

O: Oxygen

Si: Silicon

Ti: Titanium

CHAPTER 1
INTRODUCTION

More than twenty years after the last Apollo mission, the thermal history of the lunar highlands remains an unsolved puzzle. Part of the captivating mystery surrounding this heavily pock-marked terrain lies in its antiquity. An important and poorly understood rock type found in the ancient highlands is called "feldspathic granulitic impactites" (Warner et al., 1977). Early studies (e.g., Kirsten and Horn, 1974; Turner and Cadogen, 1975) of some highlands breccias reveal that the impactites are among the oldest rocks found on the Moon, dating prior to the Nectarian cataclysm. These impact breccias contain many of the clues to the Moon's complicated history. What was the thermal environment of the highlands area before the formation of the maria? What heat source was responsible for the formation of the granulitic impactite breccias and was it of global extent? What was the impact history for the Moon prior to the Nectarian cataclysm? These are but a few of the questions which remain to be resolved. My goal for this thesis has been to investigate the thermal and selenologic setting of these intriguing rocks, with inferences toward the overall thermal environment of the Moon.

Bulk compositions of the breccias resemble those of estimated average highlands crust (Taylor, 1975, 1982). Most feldspathic granulitic impactites are interpreted to be polymict breccias composed of impact melts, metamorphosed clasts, and pristine rocks (Lindstrom and Lindstrom, 1986). Chemical features of the impactites led Warner et al. (1977) to suggest that the precursor lithologies were mainly plutonic, and perhaps cumulate, rocks.

1

Most of the granulitic impactites have 70-80 % modal plagioclase and variable mafic mineral assemblages and compositions (Warner et al., 1977; Bickel and Warner, 1978; James et al., 1980). The breccias tend to fall into two broad compositional groups: ferroan and magnesian (Warren and Wasson, 1977). Lindstrom and Lindstrom (1986) further subdivided them into four groups representing a range in Fe/Mg ratios. The rocks have moderate to high concentrations of siderophile elements, indicative of meteoritic contamination (Morgan et al., 1976; Morgan and Petrie, 1979). Relatively low concentrations of REE and incompatible elements in the breccias (Hubbard et al., 1974; Blanchard et al., 1977) suggest they are essentially KREEP-free.

There have been several interpretations for the formation of rocks in the granulitic impactite suite. Hollister (1973) and Ashwal (1975) interpreted several of the samples as igneous rocks. In contrast, McGee et al. (1978) stated that the granulitic impactites had textural and chemical characteristics consistent with prolonged annealing at high temperatures. This annealing episode has been termed "Apollonian" metamorphism by Stewart (1975). The lunar samples analyzed in this study are not in the "Apollonian" class. Rather, they are what Warner et al. (1977) suggest are post-Apollonian rocks that experienced a shorter duration of metamorphism than the "Apollonian" rocks. The physical setting for this metamorphic event is still uncertain. One suggested setting is under a hot ejecta blanket (McGee et al., 1978). Studies of the Ries impact by Miller and Wagner (1979) showed that peak, post-shock temperatures in high-temperature breccias were only in the range of 500-600°C for a short time. The impact breccias from Apollo 16 and 17 are thought to have undergone metamorphism at temperatures near 1000°C for long periods of time (Warner et al., 1977). Since

hot ejecta blankets do not have peak temperatures near $1000^{\circ}C$, they are an unlikely heat source.

There are a number of obscuring factors that make it difficult to unravel the history of these breccias. One complicating factor is that there are at least two significantly different textural types (Cushing et al., 1992): poikilitic varieties which may have crystallized from an impact-induced melt, and granoblastic rocks which formed by solid-state metamorphism. These will be described in more detail in the Petrography section. Another enigmatic feature is the number of impact events that affected each breccia. A number of researchers have investigated this problem (e.g. Grieve et al., 1975; Hörz et al., 1976; Dence et al., 1976; Warner et al., 1980) and have made estimates of minimum impact events from breccia-in-breccia relationships. However, caution is advised because secondary impacting from primary excavation processes can also produce the breccia-in-breccia textures (Dence et al., 1976).

This thesis comprises the study of 24 polished lunar thin sections from the Apollo 15, 16, and 17 missions. The main purpose of this study is to unravel the thermal history for these rocks. Following the Analytical Methods section, I will describe the petrographic characteristics of the thin sections and propose a classification scheme based on three textural groups. Then, I will briefly canvass theories associated with grain growth and crystal size distribution. The Results section of this thesis begins with a discussion of 2-pyroxene equilibration temperatures for the lunar rocks. These temperatures and the depth of burial will be used to infer the heat source(s) for metamorphism of the granulitic impactites.

I will then discuss the results of crystal size distribution (CSD) measurements. CSD's can provide information about kinetics and grain growth (Marsh, 1988; Cashman and Ferry, 1988), and can be used to distinguish

3

quantitatively types of metamorphism (e.g., regional versus contact). This constrains the duration of cooling and, therefore, the thermal setting. This is the first application of the CSD approach to extraterrestrial materials.

The thesis concludes with a discussion of possible selenologic settings for the granulitic impactites and a proposal that two of the rock groups (granoblastic and poikilitic II) were metamorphosed for a relatively short time at the base of a crater, underneath fallback ejecta and impact melt. The rocks of the third group (poikilitic II) are proposed to have been impact melts.

4

CHAPTER 2
ANALYTICAL METHODS

The samples in this study are polymict impact breccias. Clast lithologies range from anorthosite to troctolite and norite, but bulk compositions are anorthositic norite. They occur at most of the Apollo highlands sites as hand samples, rake samples, and clasts in highlands breccias. They have also been found in lunar meteorites from unknown lunar sites (Taylor et al., 1991). The thin sections studied in this project are from the Apollo 15, 16, and 17 missions. Table 1 lists the compositional groups, textural types, and previous studies of the impact breccias.

Petrography and Mineral Compositions

The thin sections of the breccias were examined petrographically with a light-optical microscope under transmitted and reflected light for modes, textural relationships, and grain morphology. All mineral compositions were obtained on an automated SX-50 Cameca electron microprobe. Operating conditions were 15 keV accelerating voltage and 20 nA probe current with a fully focused beam. On-line ZAF corrections were applied to the analyses. The setups for pyroxene and olivine are presented in Appendix A. The background counting times were half of those for the peak. X-ray and backscatter imaging using the "Fast Acquisition" task also were utilized for areas of interest.

Table 1. Granulitic Impactites

Sample Number †	Compositional Group Ab	Texture £	Previous Studies
15418,19 ,98	strongly ferroan	g	a, b, t, Ab, Aj
60035,17		p I	c
67215,5	strongly ferroan	p I	d, Aa, Ab, Ae
67415,16 ,113	strongly magnesian	p I	d, i, u, Ab, Ac, Ad
67915,221		g	d, f, i, j, n, p, r, Ac, Ag
67955,52	strongly magnesian	p I	d, g, k, r, t, Ab, Ac, Af
72559,6 ,10		p II	e
73215,29 ,336 ,337 ,339		p II	f, g, o, u, Ai, Ak, Al
76230,11	moderately magnesian	p I	g, t, Ab
76235,17	moderately magnesian	p I	g, Ab, Ah
77017,160 ,161	moderately ferroan	p I	g, l, o, q, s, t, y, Ab, Af
78155,103 ,104	moderately ferroan	g	g, i, m, t, x, y, Ab
78527,4		p II	e
79215,17 ,52	moderately magnesian	g	f, g, h, v, z, Ab, Ai

Previous studies are: **a**, Richter, D. et al. (1976); **b**, Stettler, A. et al. (1973); **c**, Warner, R.D. et al. (1980); **d**, Stoffler, D. et al. (1985); **e**, Nehru, C.E. et al. (1978); **f**, Steele, I.M. et al. (1980); **g**, Warner, J.L. et al. (1977); **h**, Smith, J.V. et al. (1980); **i**, Wanke, H. et al. (1976); **j**, Rose, H.J. et al. (1975); **k**, Hollister, L.S. (1973); **l**, Uhlmann, D.R. et al. (1981); **m**, Turner, G. and Cadogan, P.H. (1975); **n**, Weiblen, P.W. et al. (1980); **o**, Laul, J.C. et al. (1974); **p**, Marti, K. et al. (1983); **q**, McCallum, I.S. et al. (1974); **r**, Nord, G.L. et al. (1975); **s**, Hodges, F.N. and Kushiro, I. (1974); **t**, Hubbard, N.J. et al. (1974); **u**, Bickel, C. E. and Warner, J.L. (1978); **v**, Bickel, C.E. et al. (1976); **x**, Bickel, C.E. (1977); **y**, Nunes, P.D. et al. (1975); **z**, McGee, J.J. et al. (1978); **Aa**, McGee, J.J. (1988); **Ab**, Lindstrom, M.M. and Lindstrom, D.J. (1986); **Ac**, Lindstrom, M.M. and Salpas, P.A. (1981); **Ad**, Lindstrom, M.M. et al. (1977); **Ae**, Lindstrom, M.M. and Salpas, P.A. (1983); **Af**, Ashwal, L.D. (1975); **Ag**, Ebihara, M. et al. (1992); **Ah**, Cadogan, P.H. and Turner, G. (1976); **Ai**, Blanchard, D.P. et al. (1977); **Aj**, Christie, J.M. et al. (1973); **Ak**, Dence, M.R. et al. (1976); **Al**, James, O.B. and Hammarstrom, J.G. (1977)

† Thin section number is designated by , (e.g., 19 in 15418,19).

£ g: granoblastic; p I: poikilitic I; p II: poikilitic II

2-Pyroxene Thermometry

For the two-pyroxene thermometry, adjoining high-Ca and low-Ca pyroxene pairs were analyzed. The mineral compositions were then applied to the Kretz (1982) and Lindsley and Frost (1992) thermometers.

Zoning Profiles

The edges and centers of the largest 3-5 unblemished grains of olivine and pyroxene were analyzed. If there was a difference in concentration of >0.15% for MgO, FeO, or CaO between the two edges and center of a grain, a profile across that grain was analyzed. Only one olivine grain in sample 15418 was found to be zoned in CaO. Since this is the only observed zoned grain among all the samples and due to the heterogeneity of lithologies, further consideration was not given to that particular profile.

Crystal Size Distribution (CSD)

Photomicrographs

Photomicrographs of granoblastic samples 79215,52 and 67915,221 were used as the primary method of obtaining crystal size distributions. The thin sections were photographed under transmitted, plane-polarized light. Methods similar to those of Marsh (1988) and Cashman and Ferry (1988) were followed. For both samples, over one thousand mafic grains (olivines and pyroxenes) were measured with a metric ruler along the greatest length of the grain. The measurements were then binned into 5 μm and 6.3 μm intervals for 79215 and 67915, respectively. The applications of grain size distributions are outlined in the CSD Theory section of the paper.

Image Processing Software

X-ray elemental (Ca, Fe, Mg, Si) and backscatter images of granoblastic sample 79215,52 were obtained on the electron microprobe. The operating conditions were 15 keV accelerating voltage and 10 nA probe current with a beam size of 5 μm. The magnification was set at 63x, the time per step was 50 milliseconds, and the step size was 5 μm. The backscatter image (Figure 1) gave the most contrast between the mafic grains and plagioclase and was incorporated into the Macintosh-based software program, *NIH Image*, version 1.44. The purpose was to determine if the use of *NIH Image* is an accurate and efficient way of measuring large numbers of grains. Prior to analyzing the grain size, a density slice was applied to the backscattered image to distinguish olivine and pyroxene from plagioclase. "Analyze Particles," under the Analyze menu, was used to obtain an automatic analysis of the grain circumferences. The advantage is that the grain sizes of numerous grains (> 2000) can be acquired in less than a minute. Assuming the grains in thin section view to be roughly circular, the diameter could then be calculated. The procedure outlined in the Photomicrographs section was then applied to the software measurements. The results are compared to the CSD of the same area procured by manual measurement in a later chapter.

8
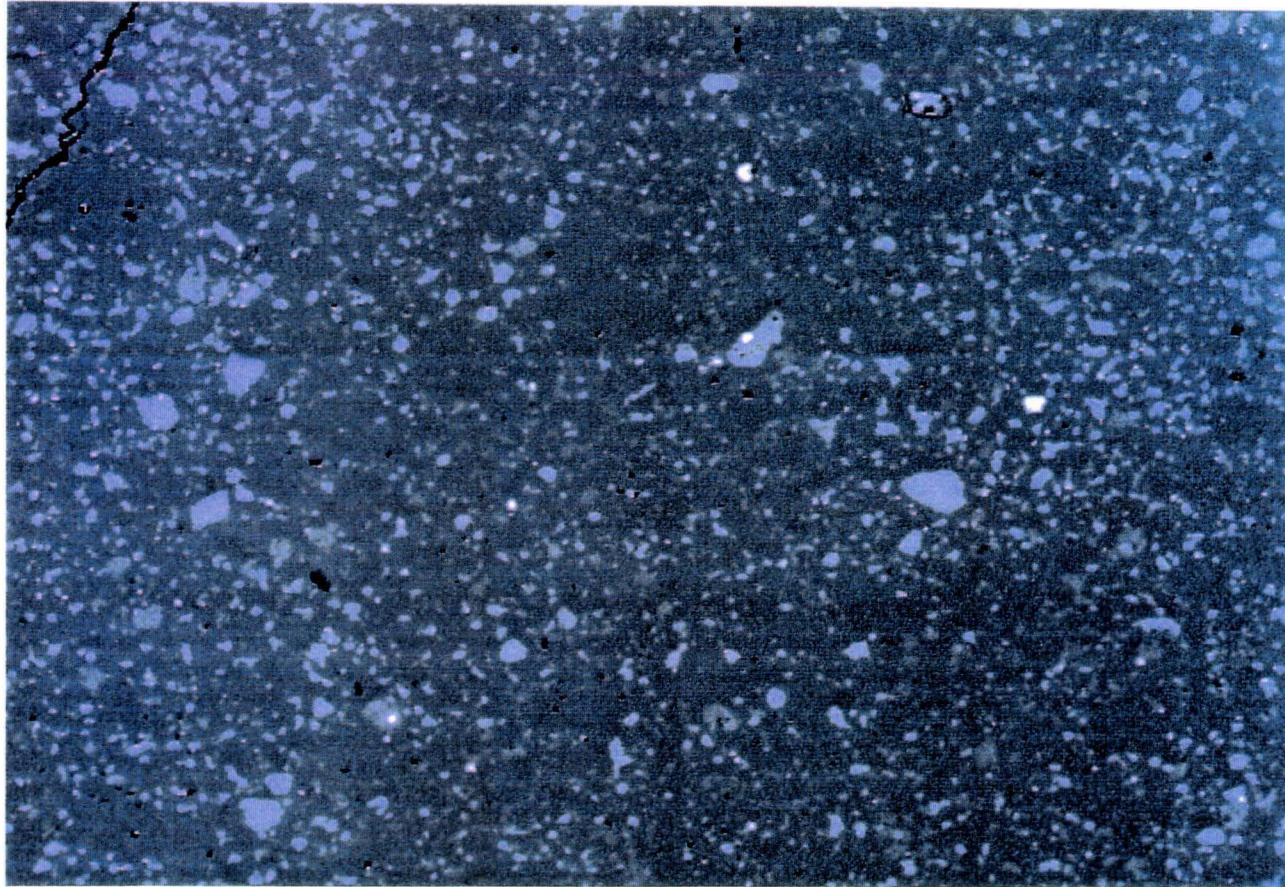
Figure 1. Backscattered image of 79215,52. Dark grey represents plagioclase, medium grey is pyroxene, light grey is olivine, and white is Fe-Ni metal. Black spots are holes, and the black line in the upper left of the image is a crack.
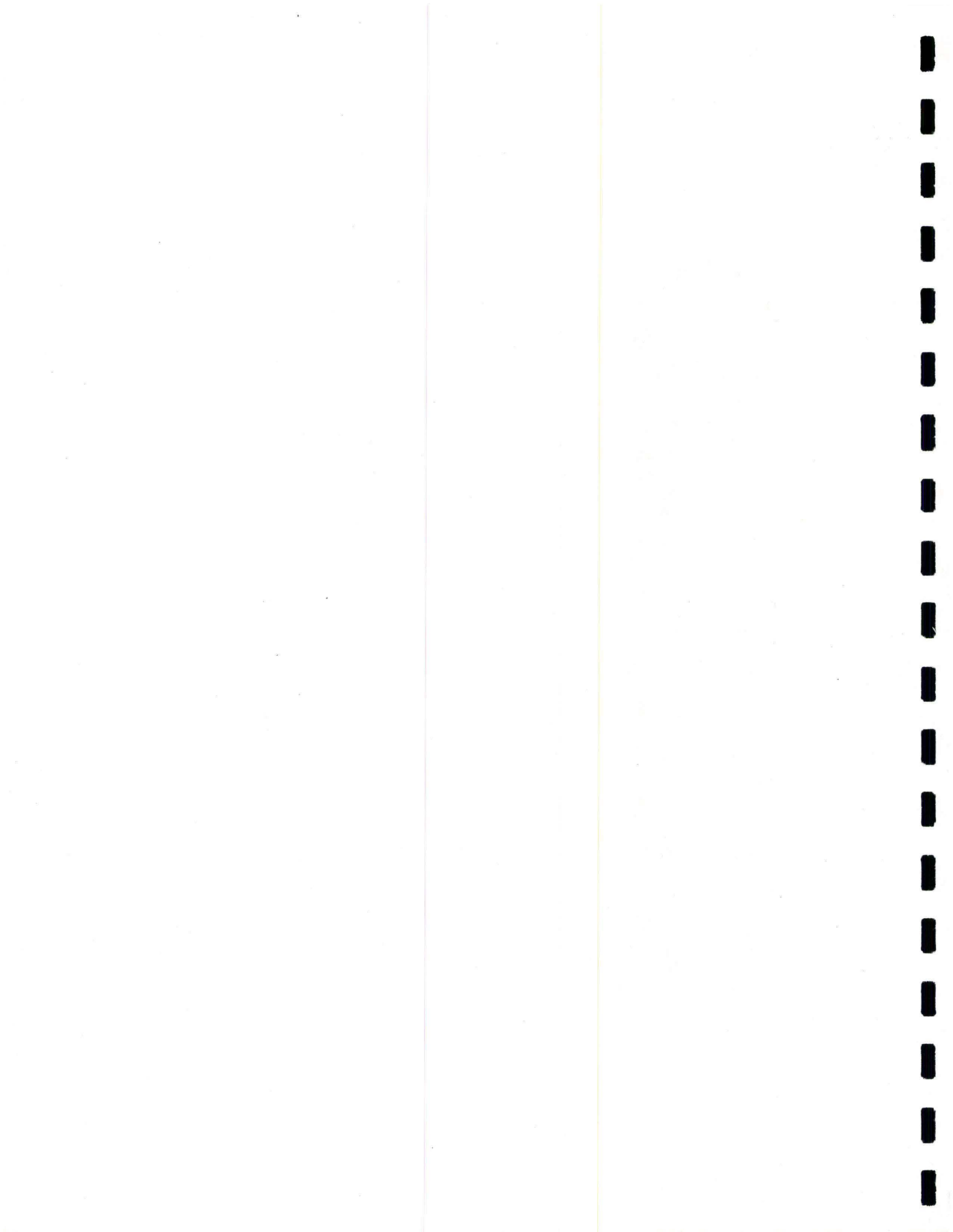
CHAPTER 3
GRAIN GROWTH AND CSD THEORY

Ostwald Ripening

The metamorphism of rocks in the granulitic impactite breccias is poorly understood. Many of the metamorphic textures (e.g. 120° junctions) seen in the granoblastic samples may be explained by diffusion and grain coarsening (Stewart, 1975). "Ostwald ripening," the growth of large grains at the expense of smaller ones, occurs during metamorphism of a polycrystalline aggregate so that the total amount of interfacial energy is reduced (Greenwood, 1969).

The increase in crystal size occurs by diffusion of material through the matrix. Within the matrix, there is simultaneous growth and dissolution of separate particles in order to reach a local equilibrium (i.e., when all the crystals are approximately the same size) (Greenwood, 1969). In an assemblage composed of various crystal sizes, only crystals with a critical radius, r^*, are in true equilibrium with the surrounding matrix. The matrix will be supersaturated with respect to particles larger than those with r^*, and those crystals will grow larger. Conversely, those crystals with $r < r^*$ will decrease in size and eventually disappear (Cashman and Ferry, 1988; Fischmeister and Grimvall, 1973). Although r^* increases with time, the *shape* of the particle size distribution when normalized to both the maximum number of crystals in any of the size bins, and the average grain diameter, remains the same (Cashman and Ferry, 1988; Markworth, 1970).

The following equations describe the Ostwald ripening process. The derivations are found in Greenwood (1969), Fischmeister and Grimvall (1973),

Martin and Doherty (1976), and Doherty (1983). In a closed system with no nucleation of new crystals, the growth rate of a crystal of radius r is related to the critical radius r^* by:

$$dr/dt = \frac{k'}{r}[1/r^* - 1/r] \tag{1}$$

where t is time and k' is a temperature-dependent constant. The critical radius is also a function of time as:

$$r^*(t)^a - r^*(0)^a = k''t \tag{2}$$

The exponent a depends on the growth mechanism. In this case, where growth is diffusion-controlled, $a = 3$ (Cashman and Ferry, 1988). The term, k'', comprises the factors which are the driving force for Ostwald ripening, namely:

$$k'' = 8v2\gamma CD/9RT \tag{3}$$

where v is the molar volume of the particle phase (4.2×10^{-6} m^3/mole for olivine), γ is the surface free energy of the particle-matrix interface (~ 1 J/m^2), C is the equilibrium concentration of solute, D is the diffusion coefficient, R is the gas constant, and T is the temperature in degrees Celsius (Fischmeister and Grimvall, 1973). Equation (2) can be rewritten as:

$$r^*(t)^3 = r^*(0)^3 + (8v^2\gamma CD/9RT)t \tag{4}$$

From this, the cooling rates for the granoblastic breccias can be extracted, leading to a better constrained thermal history for these rocks. This equation applies to isothermal annealing, but can be extended to cases where the system is cooling by repeating the calculation in small temperature increments. I used the same program used by McCoy (1990), which assumed 1°C temperature steps. Thus, t for each step in Eq. 4 is simply the inverse of the cooling rate.

Also involved in Ostwald ripening is a phenomena known as liquid phase sintering. A minute amount of melt occurs along grain edges (particularly those

11

bounded by more than three grains) and penetrates the boundaries a slight distance. Experiments in liquid phase sintering and grain growth were conducted by Jurewicz and Watson (1985). They concluded that processes identical to liquid phase sintering and Ostwald ripening of ceramic materials may occur in partially-molten systems. This would increase the rate of diffusion of elements from the matrix to the crystals, thereby allowing grains with $r > r^*$ to grow faster than simply by solid-solid diffusion. As will be shown, the granoblastic rocks did not experience much grain growth; therefore, liquid phase sintering probably did not strongly influence crystal growth. If it did operate, then the cooling rate estimates are maxima.

CSD Theory

Crystal size distributions can be shown both as a histogram of number of crystals per unit volume (N_V) versus grain size (L), and as a cumulative curve (Figure 2a, b). Linearization of the distribution data is accomplished by plotting $\ln(n)$ vs. L, where n is the slope of the cumulative curve (dN/dL), also known as the population density, or number of crystals/volume/bin (Figure 2c). From the relation of $\ln(n)$ and L, the following equations can be derived (Marsh, 1988; Cashman and Ferry, 1988):

$$n = n^0 e^{-bL} \tag{5}$$

where n^0 is the intercept at $L=0$ and b is a constant which describes the slope of the linear plot $\ln(n)$ vs. L as $b=1/Gt$, where G is the growth rate and t is the residence time for crystals in the system. N_T, the total number of crystals, is found by integrating over L:

$$N_T = \int_0^\infty n^0 e^{-bL} dL = n^0 / b \tag{6}$$

12

CRYSTAL SIZE DISTRIBUTION (CSD)

(a)

CUMULATIVE CSD

(b)
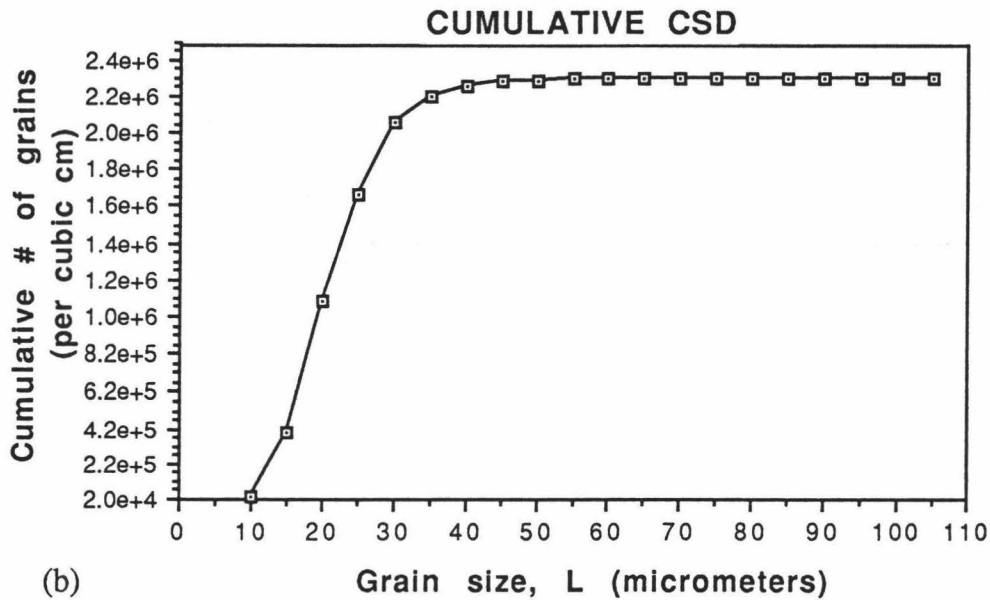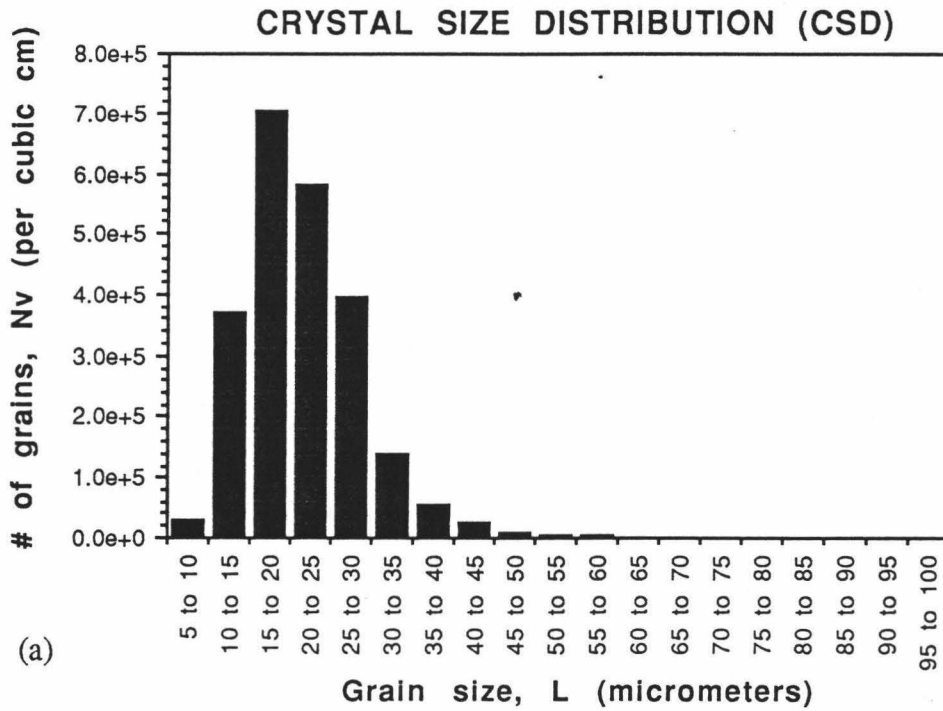
Figure 2. Crystal size distributions. (a) Nv (# of grains per unit volume) vs. L (grain size). (b) Cumulative distribution of (a). (c) Population density (ln n) vs. L.

13
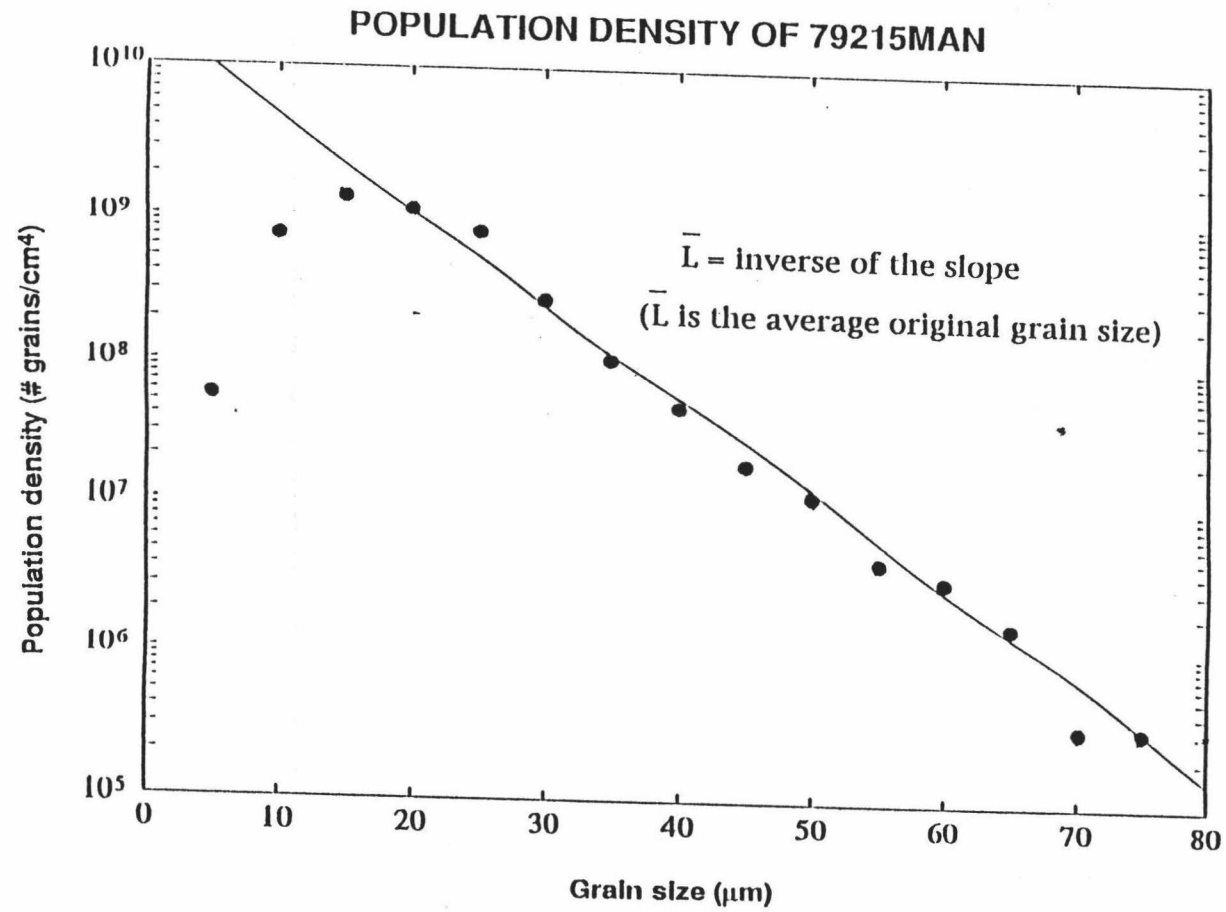
Figure 2. (Continued)

14

Likewise, L_T, the total length of all the crystals is:

$$L_T = \int_0^\infty Ln^0 d^{-bL} dL = n^0 / b^2 \tag{7}$$

The original average grain size, $\overline{L}$, can be calculated from Eq. (6) and (7):

$$\overline{L} = L_T / N_T = 1 / b \tag{8}$$

which is merely the inverse of the slope of the linear plot. While those crystals with $r > r^*$ (or $L > L^*$) of the original grain size distribution are affected by mass gained from the resorbed smaller crystals, the majority of the mass will be near L^*; therefore, the original CSD at larger sizes will not be intensely modified (Marsh, 1988).

One concern in employing CSDs for quantitative analysis is the accuracy of grain size measurements and volume estimation from area. Because grain sizes measured in thin section are always equal to or less than the actual size of the crystal, the measured distribution will always be skewed towards finer grain sizes. Cashman and Marsh (1988) and Vander Voort (1984) have addressed this issue in detail. From their experiments, Cashman and Marsh (1988) concluded that there was no more than a 10% difference in slope and intercept values between the CSD's from 2-dimensional measurements and the actual 3-dimensional CSD's. Juster et al. (1992) found that for spheres, the CSD corrected for apparent sizes is generally parallel to the uncorrected or "raw" CSD.

There are a number of different methods in converting the size distribution measured in thin section to a volume measurement (e.g. Kirkpatrick, 1977; Gray, 1978). Cashman and Marsh (1988) and Ludwig (1993) give a brief review of the various conversions and their strengths and weaknesses. To be consistent with

15

Cashman and Ferry's (1988) methods, I used the simplest conversion (e.g., Kirkpatrick, 1977):

$$N_V = (N_A)^{1.5} \qquad . \qquad (9)$$

where N_V is the number of crystals per unit volume, and N_A is the number of crystals per unit area. Kirkpatrick (1977) states that while his conversion is not entirely correct, there is no statistically consistent way of converting area measurements to volume, and that the error associated with his method is minor. Gray's (1978) conversion method, which may be more correct, also raises the number of crystals per unit area to the 1.5th power. As shown by Cashman and Marsh (1988), the slope, and hence, $\overline{L}$, is the same for both methods.

CHAPTER 4
RESULTS AND DISCUSSION

Analyses from the electron microprobe are listed in Appendix B. Equilibrium temperatures for sample 67215 were calculated using microprobe data provided by J.J. McGee.

Petrography: Textural Classification of Granulitic Impactites

The variety of textures casts a confusing facade upon an already complicated story. This confusion is in part due to the consideration of all these breccias simply as "granulites." The term 'granulite' itself is a misnomer, as even the most metamorphosed of these rocks are hornfelses, not granulites. Hornfelses are fine-grained to medium-grained granulose rocks produced by contact thermal metamorphism, whereas granulites formed by regional metamorphism at low temperatures and high pressures. Appendix B contains brief descriptions of the samples, grouped according to their texture.

Three textural types are found among the samples: poikilitic I, poikilitic II, and granoblastic. The poikilitic I rocks have an igneous-looking, almost orthocumulate texture, in which large, irregularly-shaped pyroxene oikocrysts surround subhedral to euhedral plagioclase and olivine grains (Figure 3). The term "igneous" is used here to imply a melt, but not of a plutonic or volcanic origin. The overall matrix has subangular, cataclasized grains. The poikilitic II rocks are different from the poikilitic I rocks in that the pyroxene (mostly orthopyroxene) oikocrysts are smaller and tend to be subround in shape (Figure 4); the texture may be described as poikiloblastic. The inclusions are also small
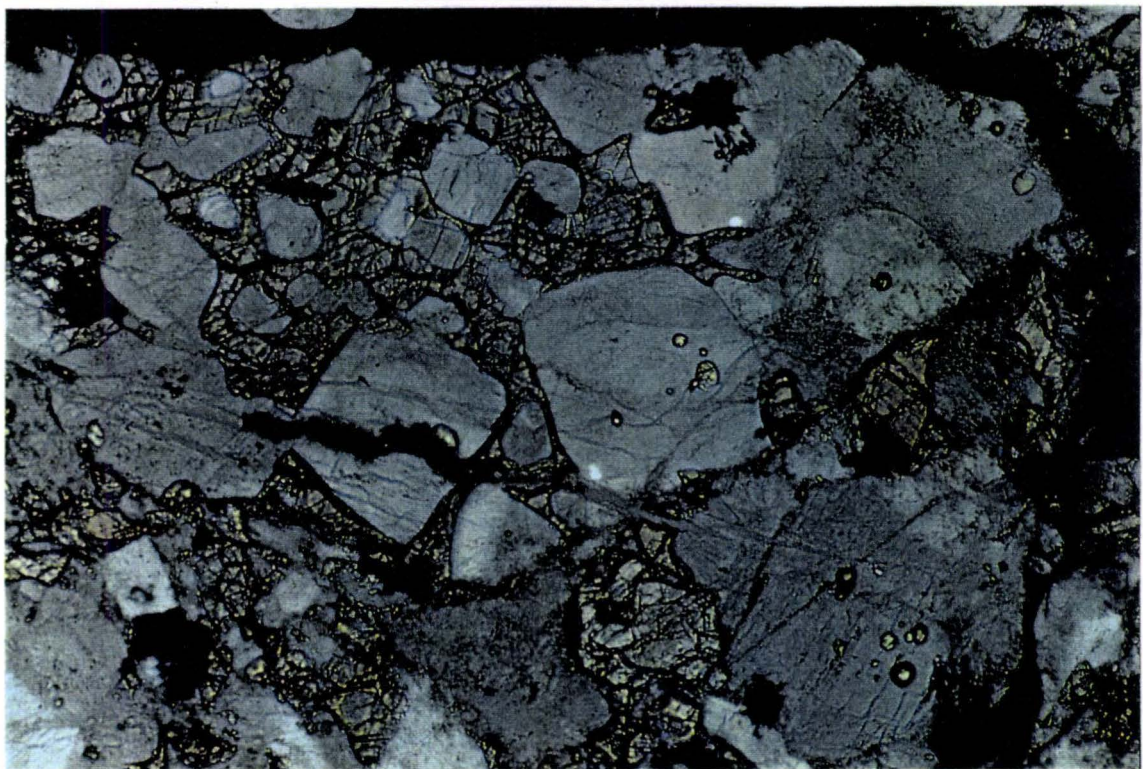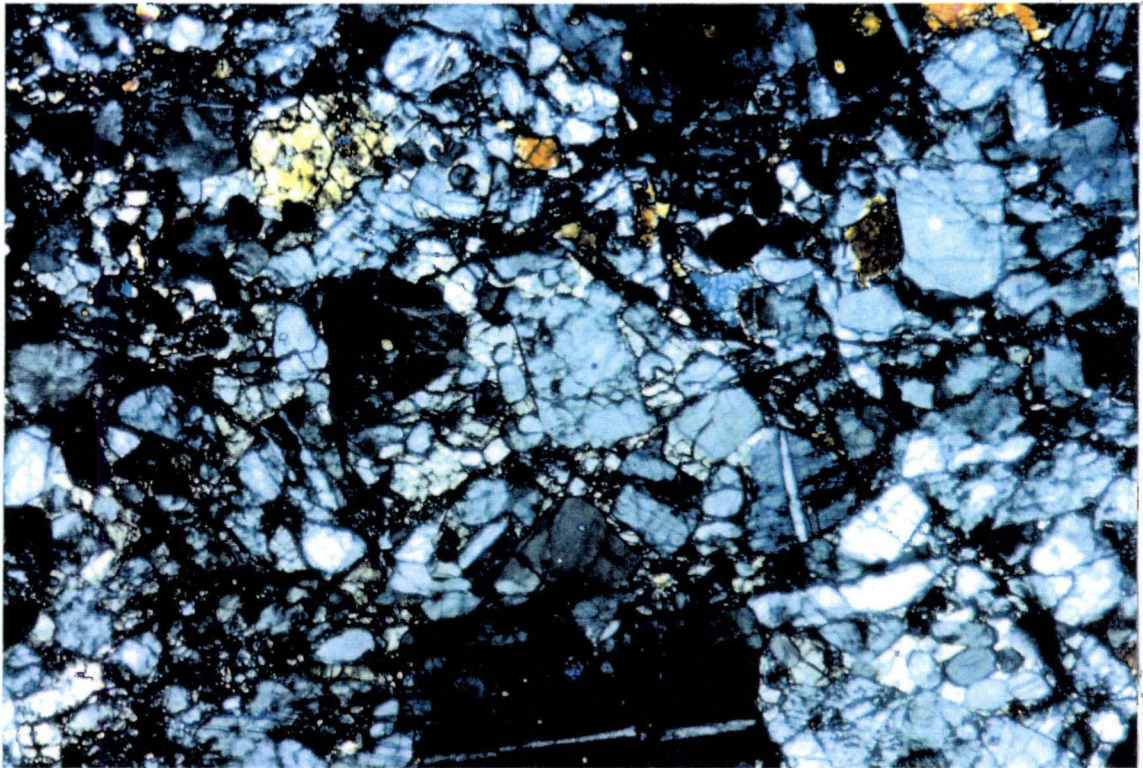
Figure 3. Poikilitic I type. Top: 77017,161 under cross-polars. Field of view is 2.6 mm across. Bottom: 77017,160 under plane polarized light. Field of view is 1.3 mm across.
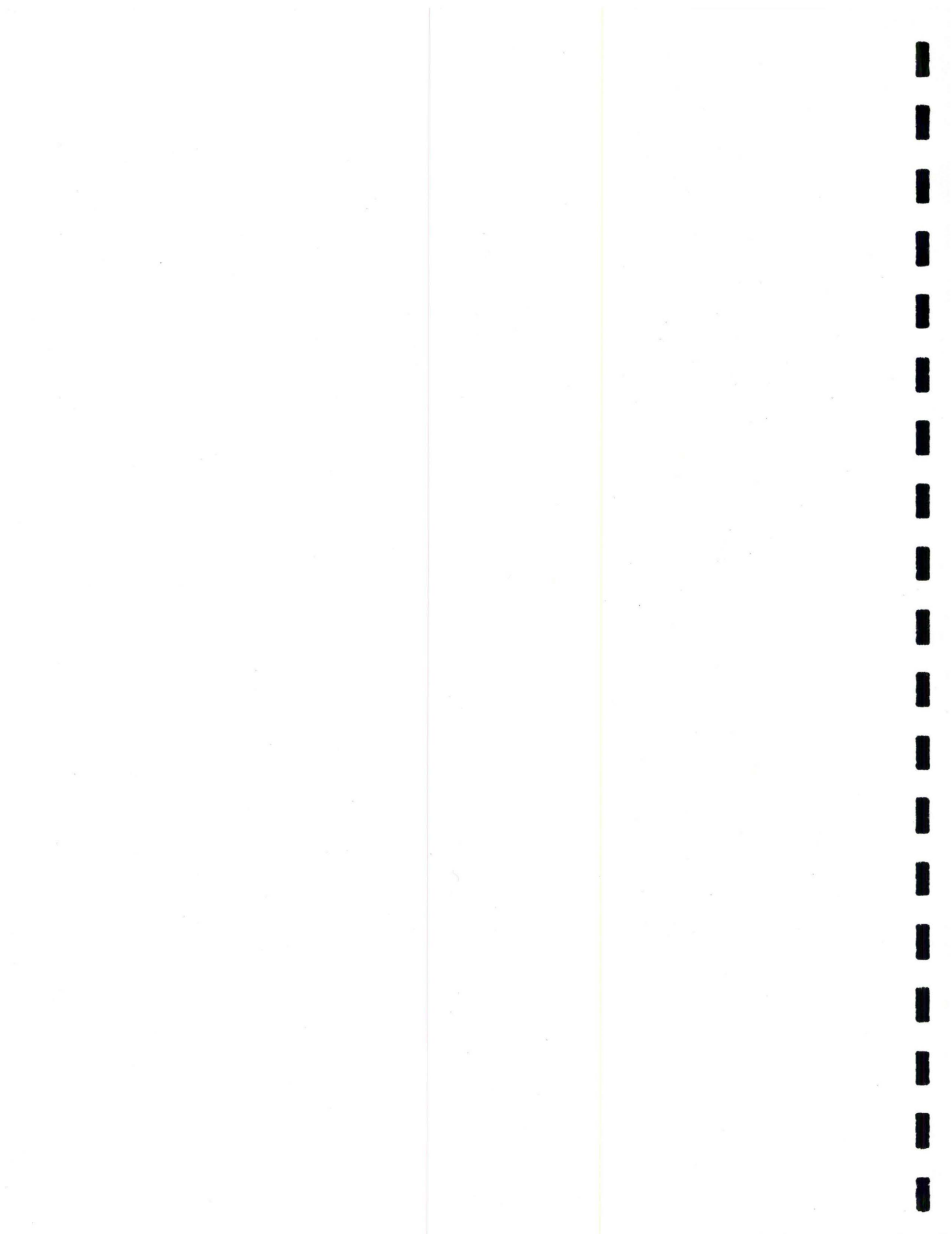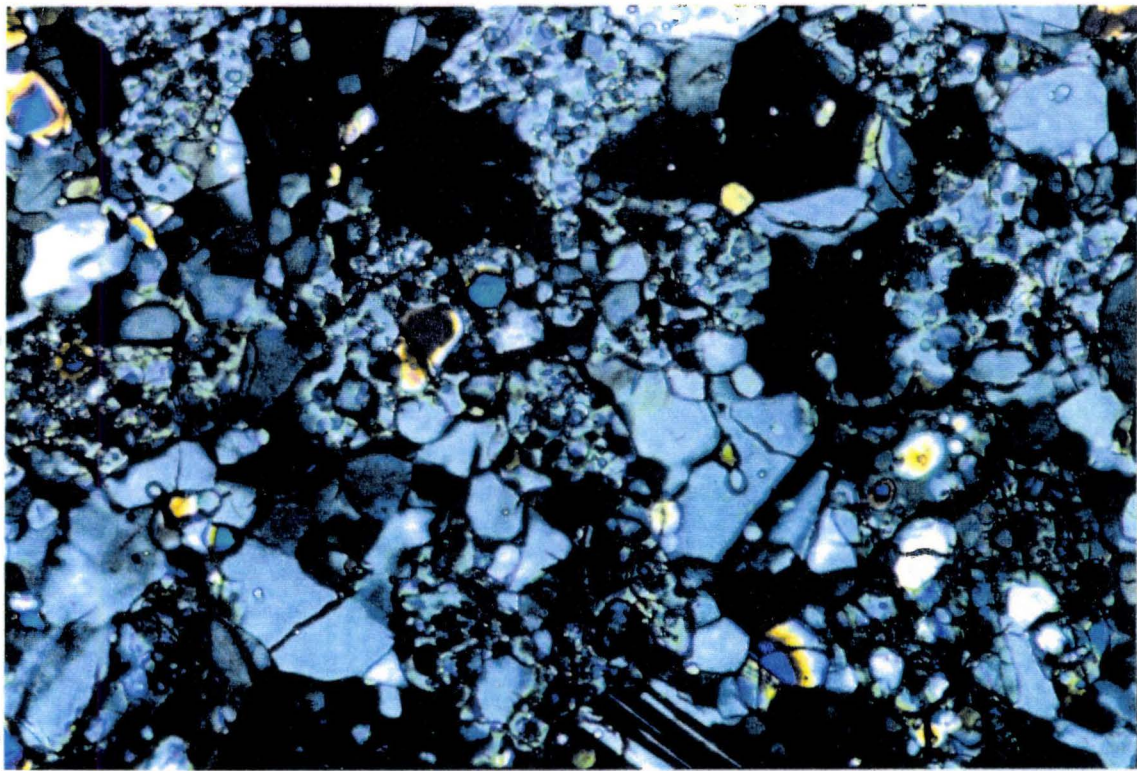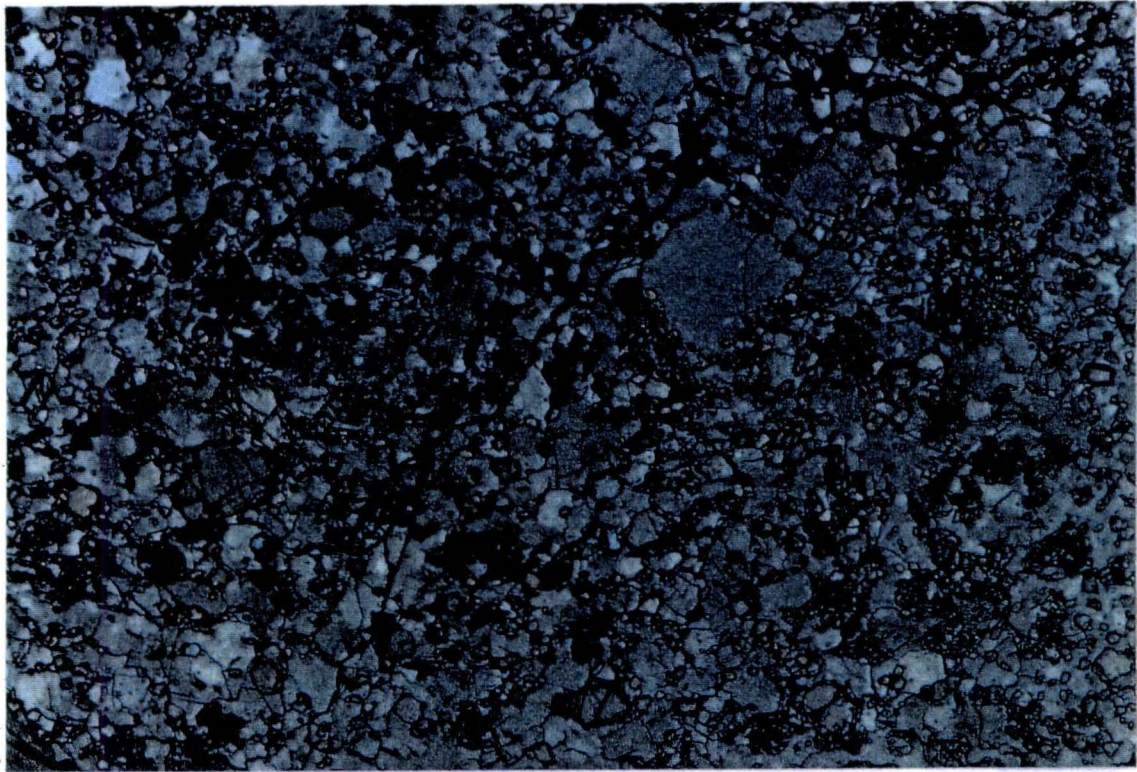
Figure 4. Poikilitic II type. Top: 72559,10 under plane polarized light. Field of view is 2.6 mm across. Bottom: 72559,10 under cross-polars. Field of view is 650 μm across.
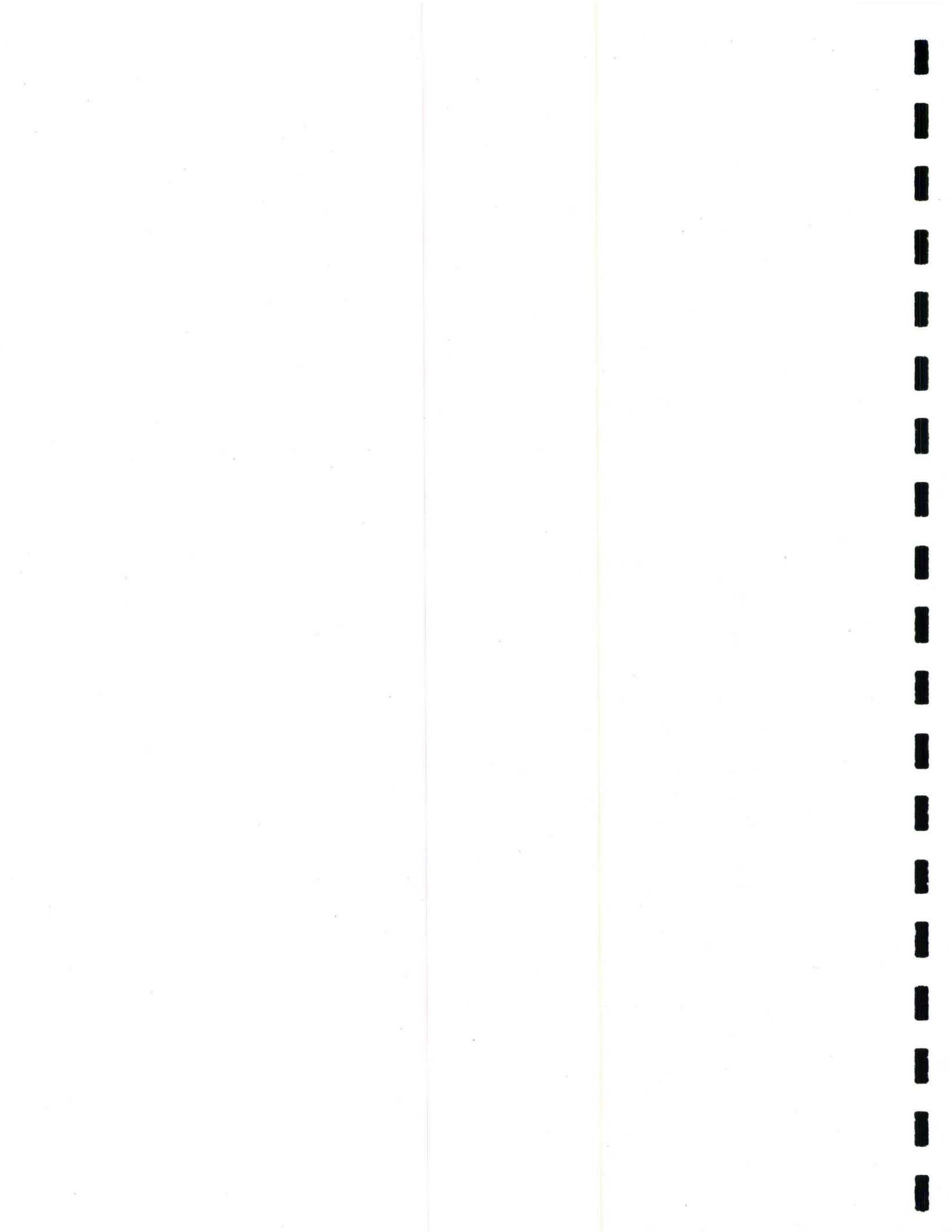
($< 15 \ \mu m$) and rounded. The matrix has a slight granular texture, with abundant quadruple junctions. The distinguishing feature of the granoblastic type is the hornfelsic relationship among the grains (Figure 5). The grains are very fine, and rounded to subrounded in shape and numerous triple junctions can be seen. A summary of the textural type characteristics is given in Table 2.

Table 2. Textural Properties of Granulitic Impactites

Granoblastic	Poikilitic I	Poikilitic II (Poikiloblastic)
—Hornfelsic texture, equant grains	—Igneous-like texture, with fine to medium-grained (0.4-1 mm) pyroxene oikocrysts and subhedral inclusions	—Oikocrysts (mostly opx) are smaller (< 0.4 mm) and less pervasive
—Very fine ($< 100 \ \mu m$) grain size	—Fine to medium grain size (50-500 μm)	—Grain size generally coarser than granoblastic rocks, but finer than poikilitic I type ($< 350 \ \mu m$)
—Abundant triple junctions	—Cataclasized	—Observe some quadruple and triple junctions; slight "granulitic look"; may be more closely related to granoblastic group

Note that the poikilitic II rocks bear a stronger resemblance to the granoblastic rocks than to those in the poikilitic I group. Grains in both the poikilitic II and the granoblastic groups are granular and subequant to equant. Also, both groups contain triple junctions, though there are more occurrences in the granoblastic rocks. Generally, grain sizes in the poikilitic II group are finer than in the poikilitic I group. The textural differences and similarities among the three groups appear to indicate that the rocks of the poikilitic I group melted,
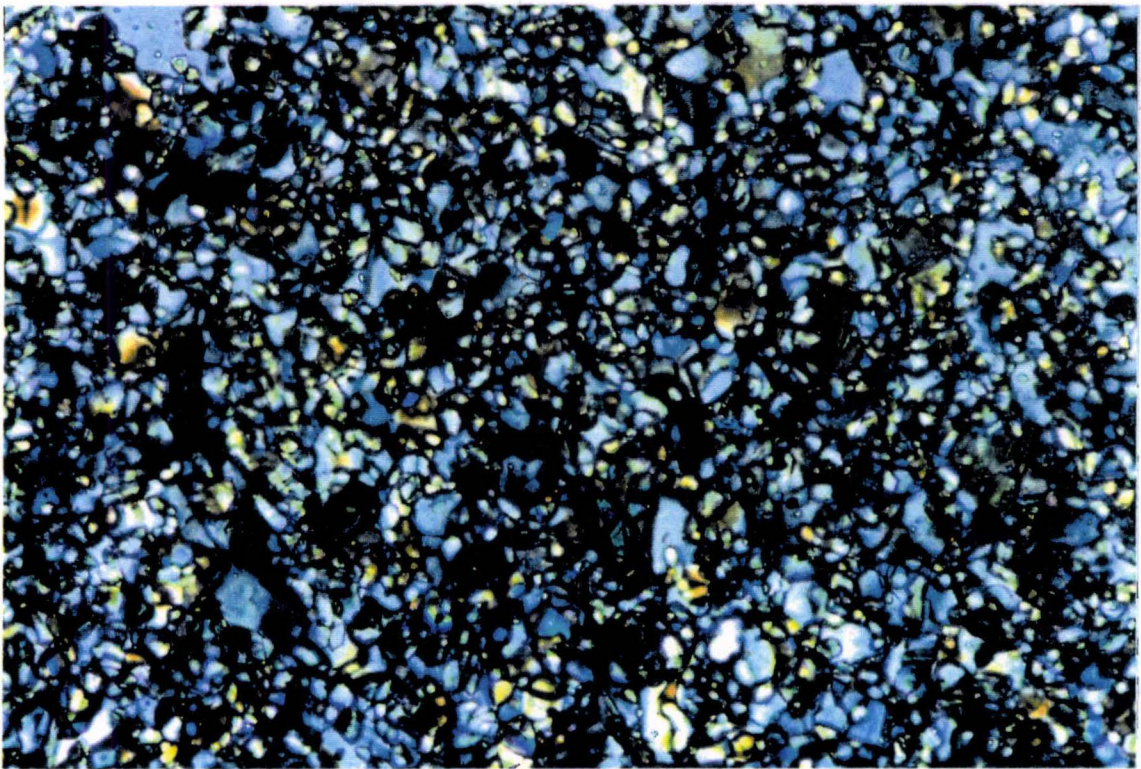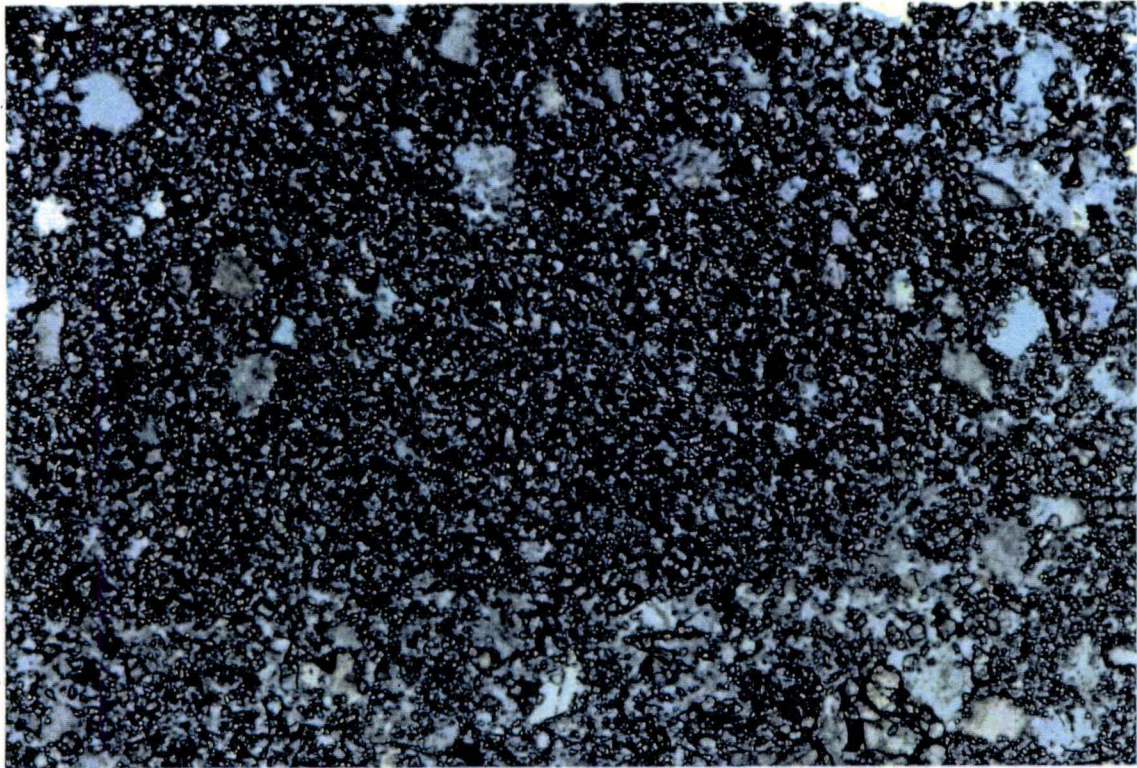
Figure 5. Granoblastic type. Top: 79215,71 under plane polarized light. Field of view is 2.6 mm across. Bottom: 79215,71 under cross-polars. Field of view is 650 μm across.

whereas rocks of the poikilitic II (poikiloblastic) and granoblastic groups were metamorphosed.

Thermometry

As stated in the introduction, 2-pyroxene equilibrium temperatures were obtained using two different methods. Below is a brief description of each method and the results.

Kretz Method

Kretz (1982) modeled the transfer and exchange reactions of Ca and the Mg:Fe ratios between high- and low-Ca pyroxenes. The thermometer involving the exchange of Fe and Mg did not produce consistent results for the lunar breccias, so only the transfer reaction for Ca was used to calculate the equilibrium temperatures. For the Ca-thermometer, a linear relation exists between ln $[En]^{Cpx}$ and $1/T$, where [En] is the mole fraction of En in pyroxene and T is temperature. However, there is a discontinuity near 1100°C, producing two equations, one for each linear segment:

Upper segment (> 1080°C):

$$T(°C)=\{1000/[0.468 + 0.246X^{Cpx} - 0.123 \ln (1 - 2[Ca]^{Cpx})]\} - 273 \qquad (10)$$

Lower segment (< 1080°C):

$$T(°C)=\{1000/[0.054 + 0.608X^{Cpx} - 0.304 \ln (1 - 2[Ca]^{Cpx})]\} - 273 \qquad (11)$$

where X is the atomic fraction $Fe^{2+}/(Mg + Fe^{2+})$ and [Ca] is the atomic fraction $Ca/(Ca + Mg + Fe^{2+})$.

The 2-pyroxene temperatures for the impact breccias are given in Table 3. Most of the samples cluster at near solidus temperatures (~1100°C) when plotted against Mg # (Figure 6). The poikilitic I breccias form a tighter cluster (with the exception of 67215) than the granoblastic samples.

22
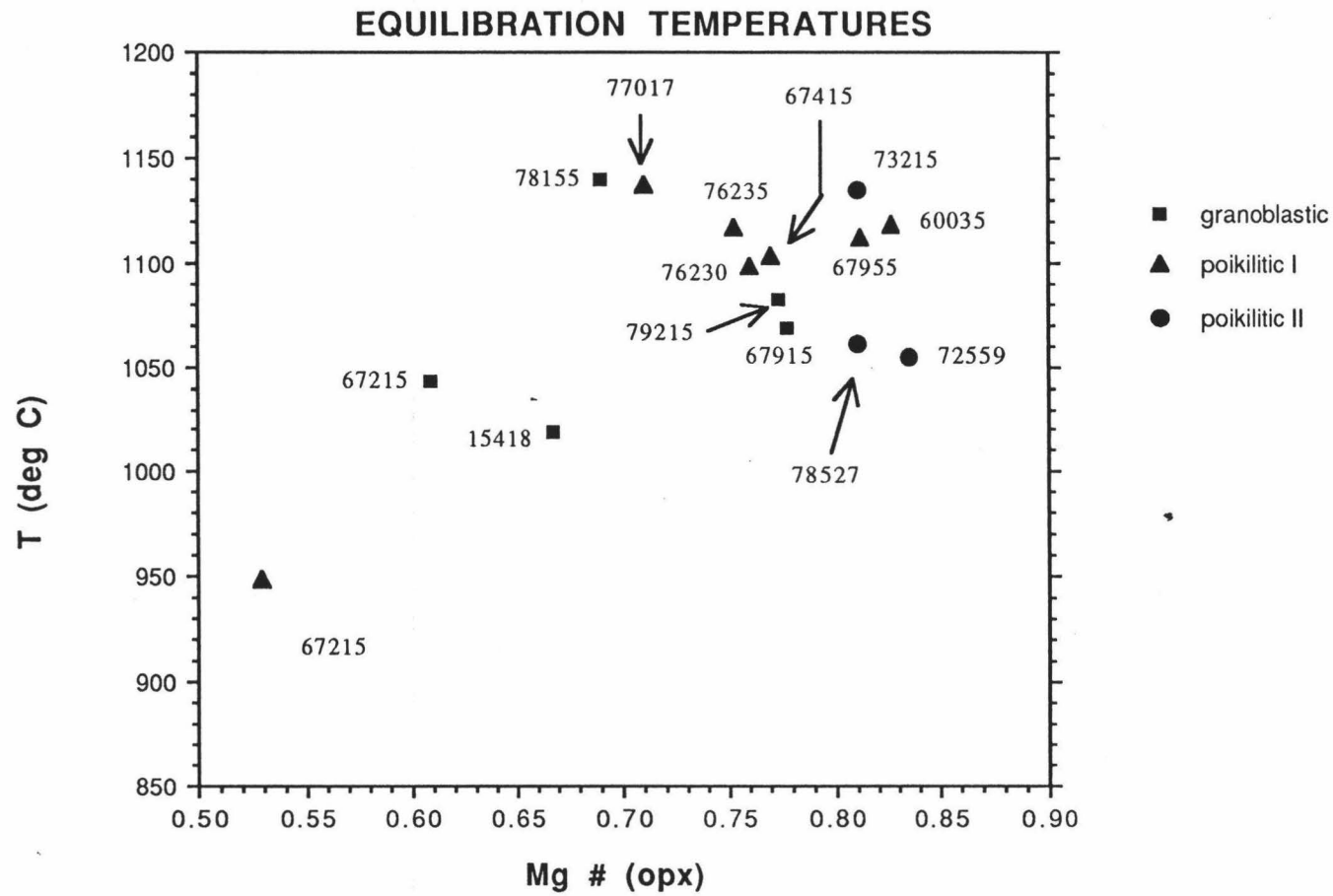
Figure 6. 2-pyroxene equilibration temperatures by the Kretz method.

23

Table 3. 2-Pyroxene Temperatures from Kretz Thermometer

Sample	Thin section and notes	Average T (°C)	Mg# (Opx)
15418	,98	1019	0.67
60035	,17	1118	0.83
67215	compositions from	949 (poik I)	0.42
	J.J. McGee	1043 (gran)	0.61
67415	,113	1103	0.77
67915	,221	1068	0.78
67955	,52	1112	0.81
72559	clast 10/1, 10/2	1055	0.84
73215	,336 ,339	1135	0.81
76230	,11	1099	0.76
76235	,17	1117	0.75
77017	,160 ,161	1137	0.71
78155	,4	1140	0.69
78527	clast 4/2	1061	0.81
79215	,71	1082	0.77

Lindsley and Frost Method—QUILF

Lindsley and Frost (1992) developed thermodynamic solution models to estimate equilibrium temperature, pressure, and oxygen fugacity. This program, involving 59 equilibria among augite, pigeonite, orthopyroxene, olivine, quartz, titaniferous magnetite, and ilmenite in $FeO-CaO-MgO-SiO_2-TiO_2$, is called QUILF (Quartz-Ulvöspinel-Ilmenite-Fayalite). A detailed explanation of QUILF comes in two parts: the theory (Lindsley and Frost, 1992) and a number of applications using the program (Frost and Lindsley, 1992). In order to compare the results from the Kretz method with QUILF, I used only the reactions involving 2 pyroxenes:

En in Aug and Opx $\quad$ $aMg_2Si_2O_6 = oMg_2Si_2O_6$
Fs in Aug and Opx $\quad$ $aFe_2Si_2O_6 = oFe_2Si_2O_6$
Di in Aug and Opx $\quad$ $aCaMgSi_2O_6 = oCaMgSi_2O_6$
Hd in Aug and Opx $\quad$ $aCaFeSi_2O_6 = oCaFeSi_2O_6$
En in Aug and Pig $\quad$ $aMg_2Si_2O_6 = pMg_2Si_2O_6$
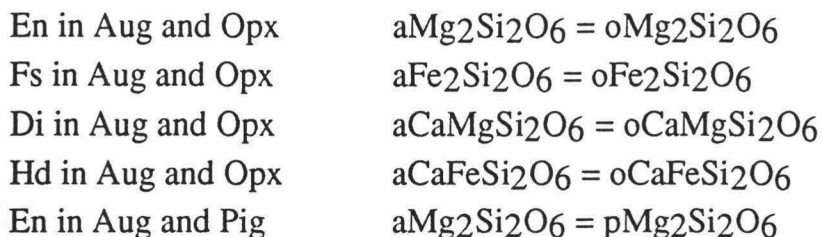
Fs in Aug and Pig	$aFe_2Si_2O_6 = pFe_2Si_2O_6$
Di in Aug and Pig	$aCaMgSi_2O_6 = pCaMgSi_2O_6$
Hd in Aug and Pig	$aCaFeSi_2O_6 = pCaFeSi_2O_6$

The program allows the user to choose which reactions to use for the calculations. Three combinations of reactions used to calculate temperature were: all components of the system (En-Fs-Di-Hd), Di-Hd, and En-Fs. The QUILF program uses Wo-En-Fs compositions specifically calculated within a subroutine, and the authors strongly advise against the use of other methods to obtain them. The pressure was set at 1 kbar, with the assumption that the lunar breccias were not deeply buried (on the Moon, 1 kbar corresponds to 20 km). The temperature was also calculated at a pressure of 1 bar and 5 kbars, with no significant difference. Oxygen fugacity does not substantially affect pyroxene equilibria, and so was ignored.

Table 4 lists the calculated temperatures using the various combinations. "Uncertainties" listed with the temperature refer to how well the pyroxenes have equilibrated with each other for the conditions and compositions given; lower values indicate better equilibration. Using all of the components for pyroxene equilibria provided temperatures closest to those of the Kretz thermometer ($\pm$ 60°) (Figure 7a). Most of the temperatures plot near 1100°C, but there is a wider range of temperatures among the samples compared to the results using the Kretz Ca-thermometer. The Di-Hd combination generally yields the highest temperatures, followed by the all-components combination, then the En-Fs reaction set (Figure 7b, c). The difference in temperature between the Di-Hd and En-Fs reactions is highly variable in all three textural types. This may suggest slight compositional heterogeneity among and within the samples. This is not entirely surprising, as most of the samples are polymict breccias.

25

Table 4. Lindsley and Frost 2-pyroxene temperatures

Sample		Average temperatures		
		All components	Di/Hd	En/Fs
15418,98		1378	1414	1287
	Uncertainty	30	46	50
60035,17		1417	1451	1314
	Uncertainty	50	35	70
67215		1269	1311	1155
		1189	1219	1101
	Uncertainty	75	58	80
67415, 113		1346	1413	1240
	Uncertainty	70	50	100
67915, 221		1367	1365	1510
	Uncertainty	50	60	100
67955,52		1351	1401	1226
	Uncertainty	50	60	77
72559,10		1367	1404	1282
	Uncertainty	50	30	44
73215, 336		1422	1457	1327
	Uncertainty	50	30	50
76230,11		1403	1428	1360
	Uncertainty	86	40	70
76235,17		1473	1557	1307
	Uncertainty	155	30	60
77017, 160,161		1545	1644	1334
	Uncertainty	120	90	112
78155,4		1283	1406	1254
	Uncertainty	107	218	107
78527,4		1296	1365	1289
	Uncertainty	37	151	8
79215,71		1326	1351	1258
	Uncertainty	37	25	48

Figure 7. 2-pyroxene equilibration temperatures by the Lindsley and Frost method. (a) Using all components, (b) Using Di-Hd components, (c) Using En-Fs components.

27

EN-FS COMPONENTS
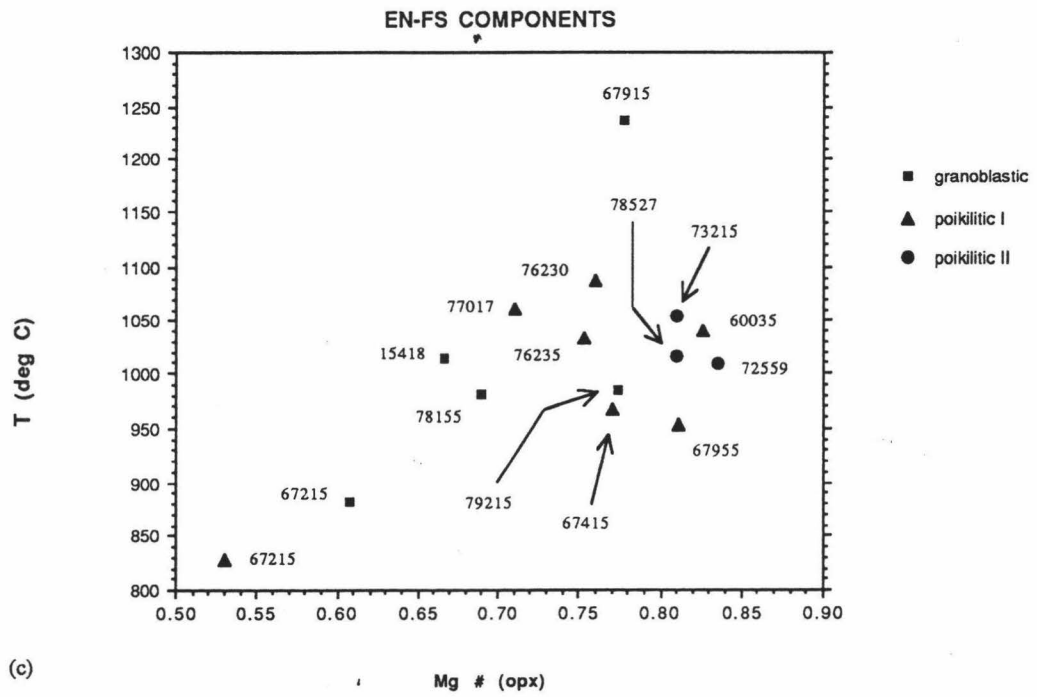
Figure 7. (Continued)

28

Nevertheless, the fact that most of the samples give results near 1100°C implies that most of the samples were equilibrated at high temperatures. This holds for both the impact melts (poikilitic I type) and metamorphosed breccias (poikilitic II and granoblastic types), suggesting that all three varieties are related to each other. The equilibration temperatures calculated by the Kretz method will be used along with the CSD results to model the duration of time for grain growth in the granoblastic samples. I use the Kretz thermometer because it is well-tested and has reliably provided reasonable temperatures for others. The two methods also give temperatures which are within 30°C (accuracy of the Kretz thermometer is ±50°C) of each other.

Crystal Size Distribution (CSD)

Photomicrographs

Two granoblastic samples were chosen for the crystal size distribution measurements, samples 79215,52 and 67915,221. These samples were chosen because the grain boundaries are easily distinguishable. The resulting CSDs show that the two samples had similar original average grain sizes and both underwent Ostwald ripening.

Histograms of N_V vs. L (Figures 8a and 9a) for the mafic minerals in 79215 (referred to hereon as 79215man to distinguish it from the CSD attained by the image processing software) and 67915 show a large number of intermediate (13.33-26.67 μm) grains and a decreasing number of large grain sizes (note differences in scale for vertical and horizontal axes). There is also an abrupt drop in the number of fine grains. Displayed as a cumulative size distribution, the curve rises rapidly, then flattens (Figures 8b, 9b). Figures 10 and 11 are plots of

29

79215MAN

(a)

Grain size, L (micrometers)

CUMULATIVE CSD—79215MAN

(b)

Grain size, L (micrometers)
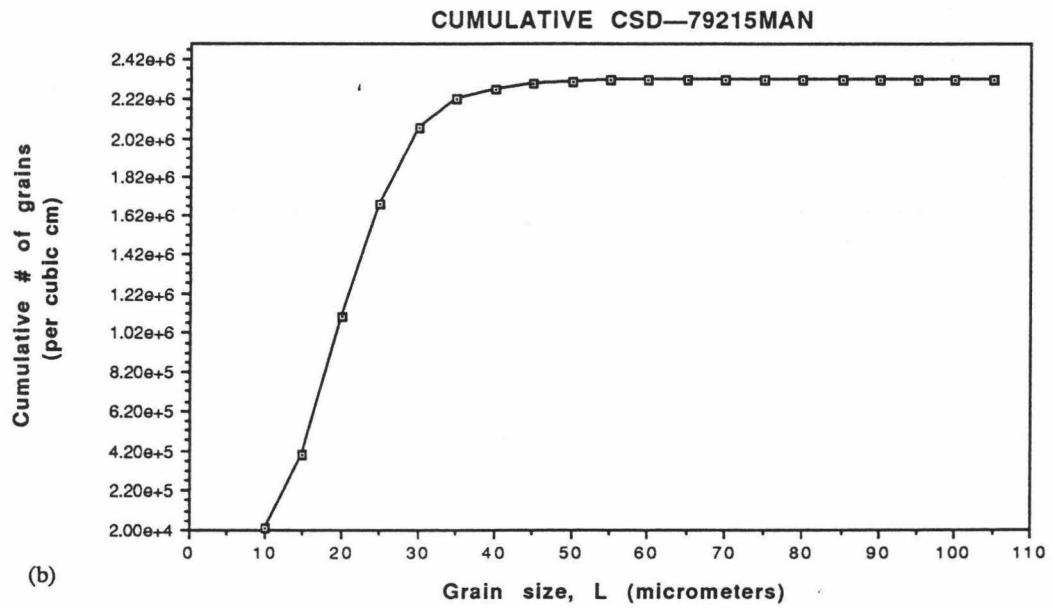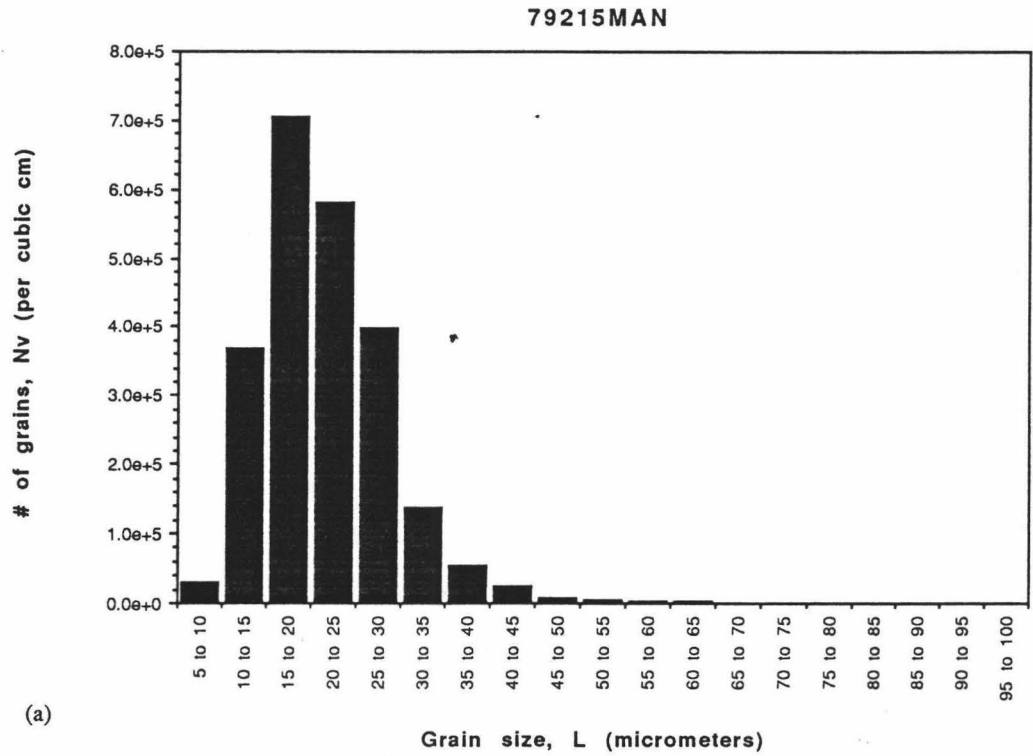
Figure 8. CSD for 79215man. (a) Binned grain size measurements,
(b) Cumulative grain size distribution.

30

CSD FOR 67915

(a)

Grain size (micrometers)

CUMULATIVE CSD FOR 67915

(b)

Grain size (micrometers)
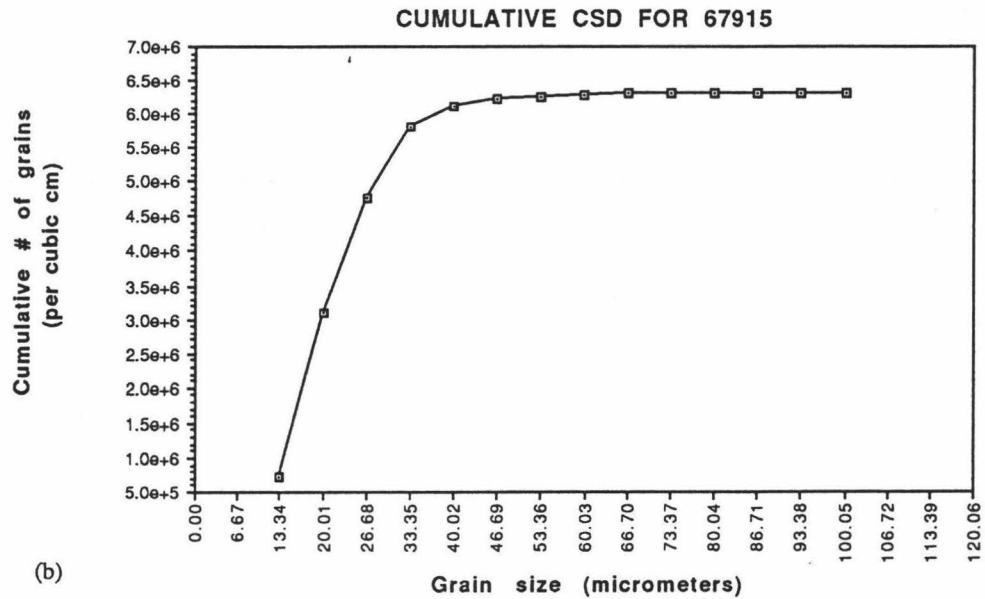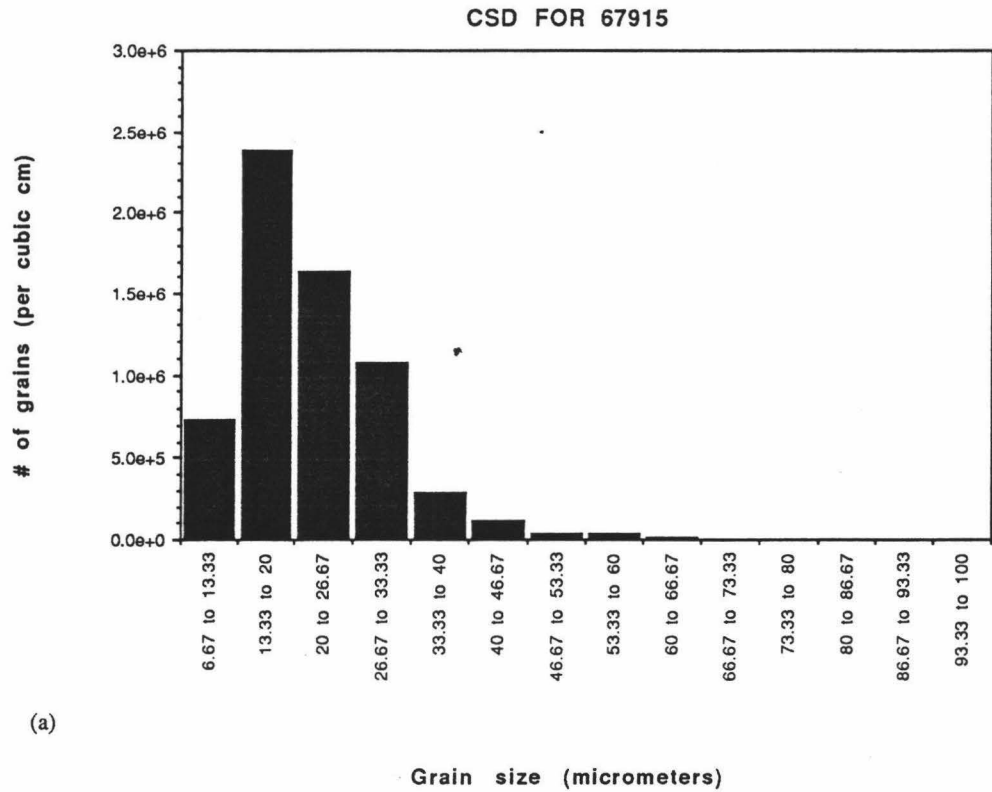
Figure 9. CSD for 67915. (a) Binned grain size distribution,
(b) Cumulative grain size distribution.

31

POPULATION DENSITY OF 79215MAN

$\overline{L} = 6.8 \ \mu m$

Grain size (μm)

Population density (# grains/cm⁴)

Figure 10.

32

POPULATION DENSITY OF 67915

$\bar{L} = 7.9 \ \mu m$

Grain size (µm)

Population density (# grains/cm^4)
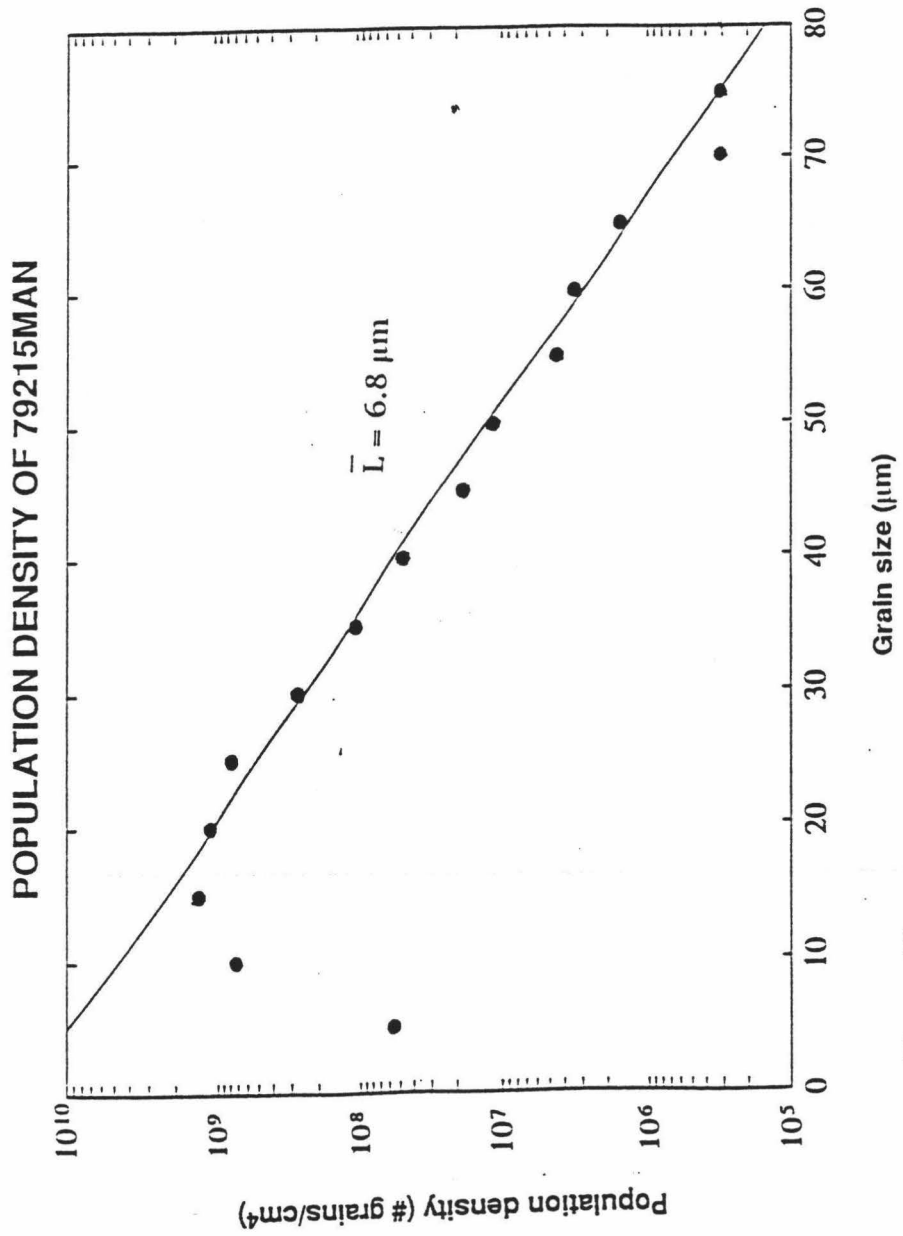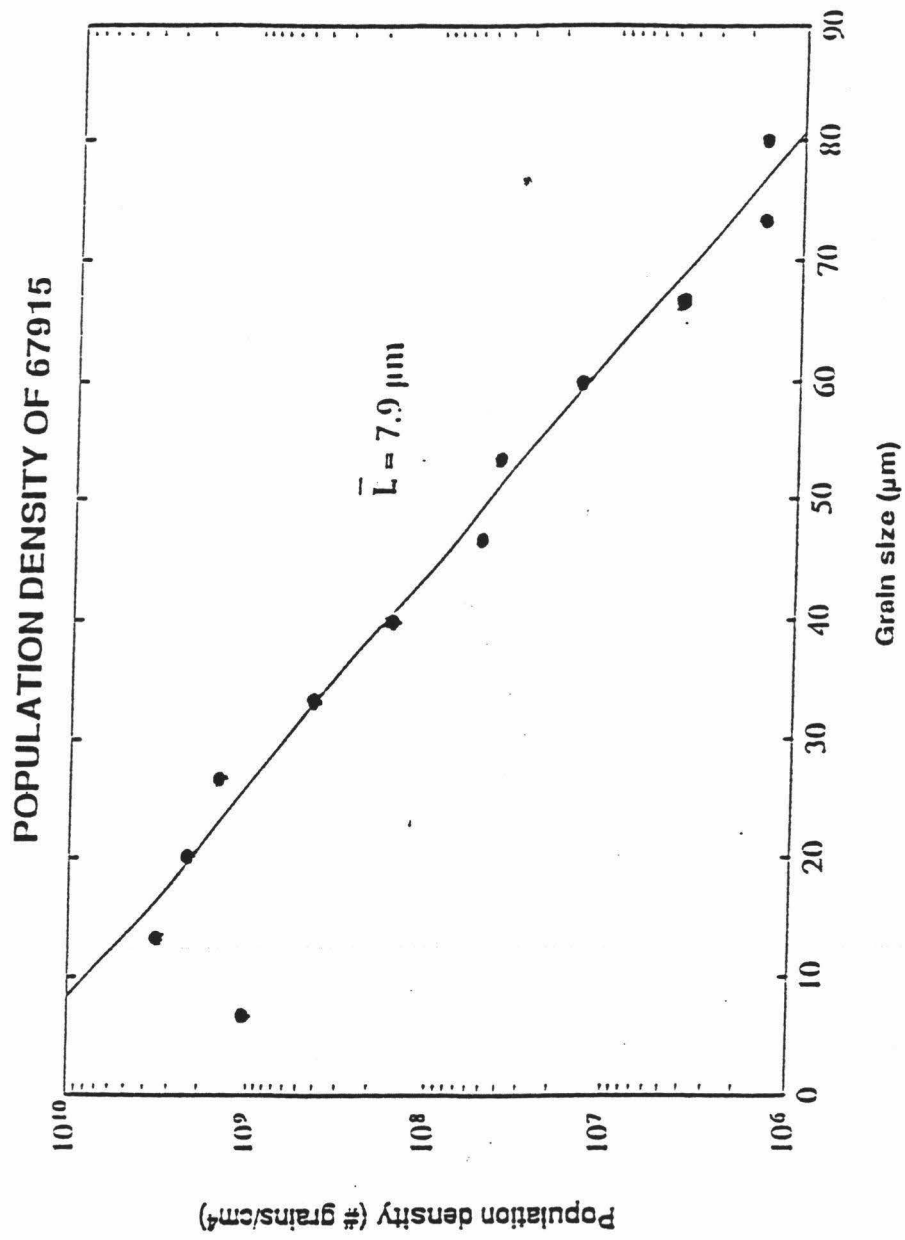
Figure 11.

ln(n) vs. L for 79215man and 67915. Both samples show an abrupt decrease in the population density for the fine grain size classes.

As discussed in the CSD Theory section of this thesis (p. 12), the inverse slope of the CSD curve provides the average original grain size. A linear regression applied to the curves result in slopes of 0.15 μm^{-1} and 0.13 μm^{-1} for 79215 and 67915, respectively. This gives average original grain sizes of 6.8 μm and 7.9 μm for the respective samples. Thus, the two granoblastic samples, though seemingly variable in overall grain size, appear to have the same original average grain size.

The sharp depletion in fine grain size classes seen in the CSDs was previously attributed to varying nucleation rates with time in terrestrial metamorphic rocks (Kretz, 1966; Jones and Galwey, 1966). However, the lunar samples were fragmented by impacts and did not nucleate. Therefore, varying nucleation rates are an unlikely explanation for the CSD shape in these rocks. A more probable explanation for the shape of the curve is that suggested by Cashman and Ferry (1989), where the linearity of the larger grain size classes represents the original size distribution and the decrease seen in the fine grain size classes is due to Ostwald ripening. The smallest grains have been preferentially dissolved by annealing.

Image 1.4 Software

Grain sizes of sample 79215,52 were measured using the image processing software, *NIH Image*. There are complications in using this program. One problem is that two or more adjoining crystals will appear as one large crystal. As such, the grains must be manually separated by drawing a boundary between the grains. A considerable amount of subjectivity is involved in deciding the proper location of the boundaries. Also, when drawing the boundary, a pixel-

34

worth (here, equal to 0.167 mm) of the grain is lost. Therefore, the resulting CSD may contain an aberrant number of fine grain size classes.

A second complication in using this program occurs when the "Analyze Particles" task is in operation. When the perimeters (circumferences) of the grains are measured, the pixel shape causes a slight increase in the actual size of round grains. The amount of the increase is dependent upon the grain size. To correct for this, circles of known circumference were measured using "Analyze Particles," and empirical correction factors were calculated. These factors were then applied to grains of various size classes (see Appendix D). However, there will still be error associated with the accuracy of the measurement.

The crystal size distribution for 79215img (Figure 12a, b) reveals a different picture from that of 79215man. As expected from the explanation above, the mode for 79215img is in the fine (9.14 μm) grain size rather than intermediate grain size category. Not evident from the histogram is the extremely sharp depletion in the very fine grain size bin (0 - 5 μm). The decrease in larger grain sizes is similar to 79215man. Due to the complications associated with distinguishing individual grains and measurement of the circumference, this particular image processing program may not be suitable for doing critical analyses of crystal size distributions of fine-grained rocks. In a plot of ln(n) vs. L (Figure 13), 79215img provides similar results to 67915. The linear regression curve for the intermediate to large size grains classes has a slope of 0.13 μm^{-1}, or 7.9 μm for the average original grain size.

Grain Growth by Ostwald Ripening

From the average original grain size obtained by the CSD data, the cooling rate was estimated assuming diffusion-controlled grain growth and using the

35

79215IMG

# of grains (per cubic cm) vs Grain size (micrometers)

(b)

CUMULATIVE CSD FOR 79215IMG

Cumulative # of grains (per cubic cm) vs Grain size (micrometers)
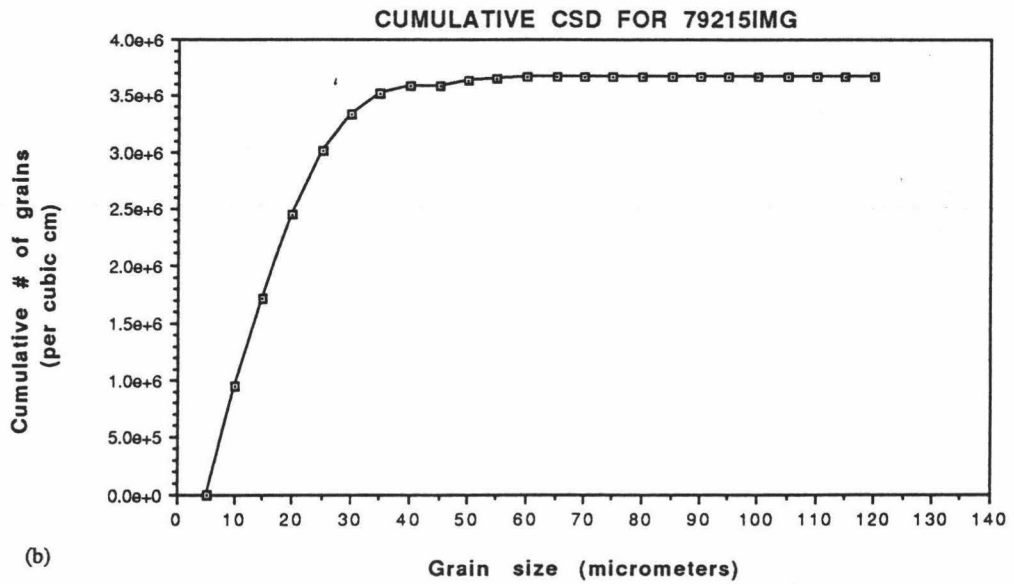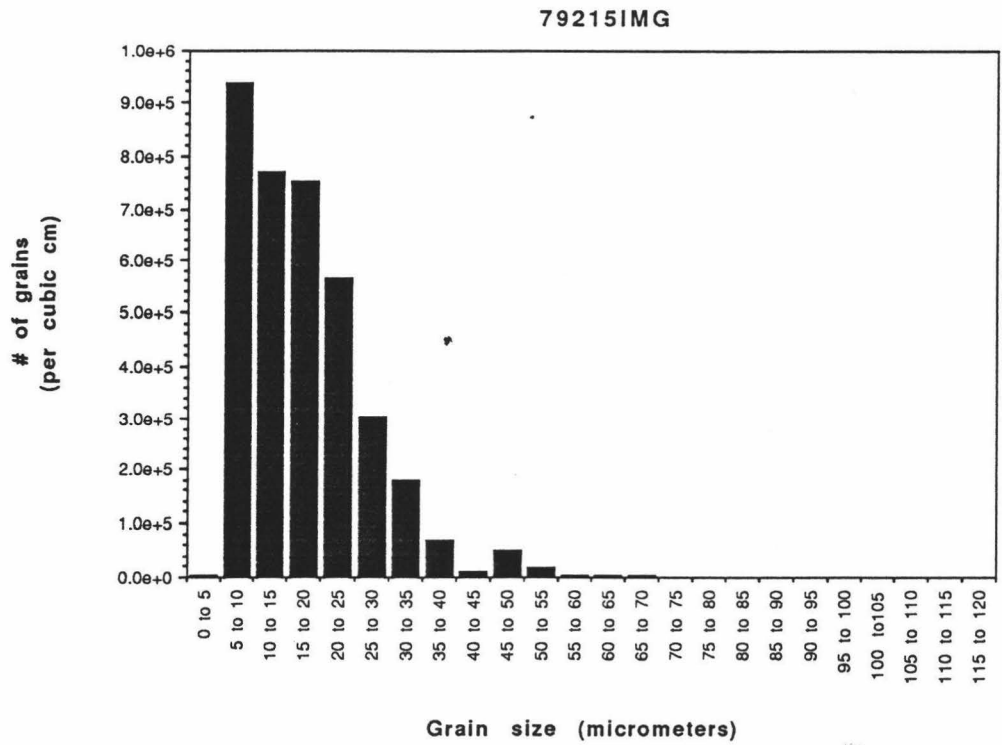
Figure 12. CSD for 79215img. (a) Binned grain size distribution, (b) Cumulative grain size distribution.

36

POPULATION DENSITY OF 79215IMG

$\bar{L} = 7.9 \ \mu m$

Population density (# grains/cm⁴)

Grain size (µm)

Figure 13.

37
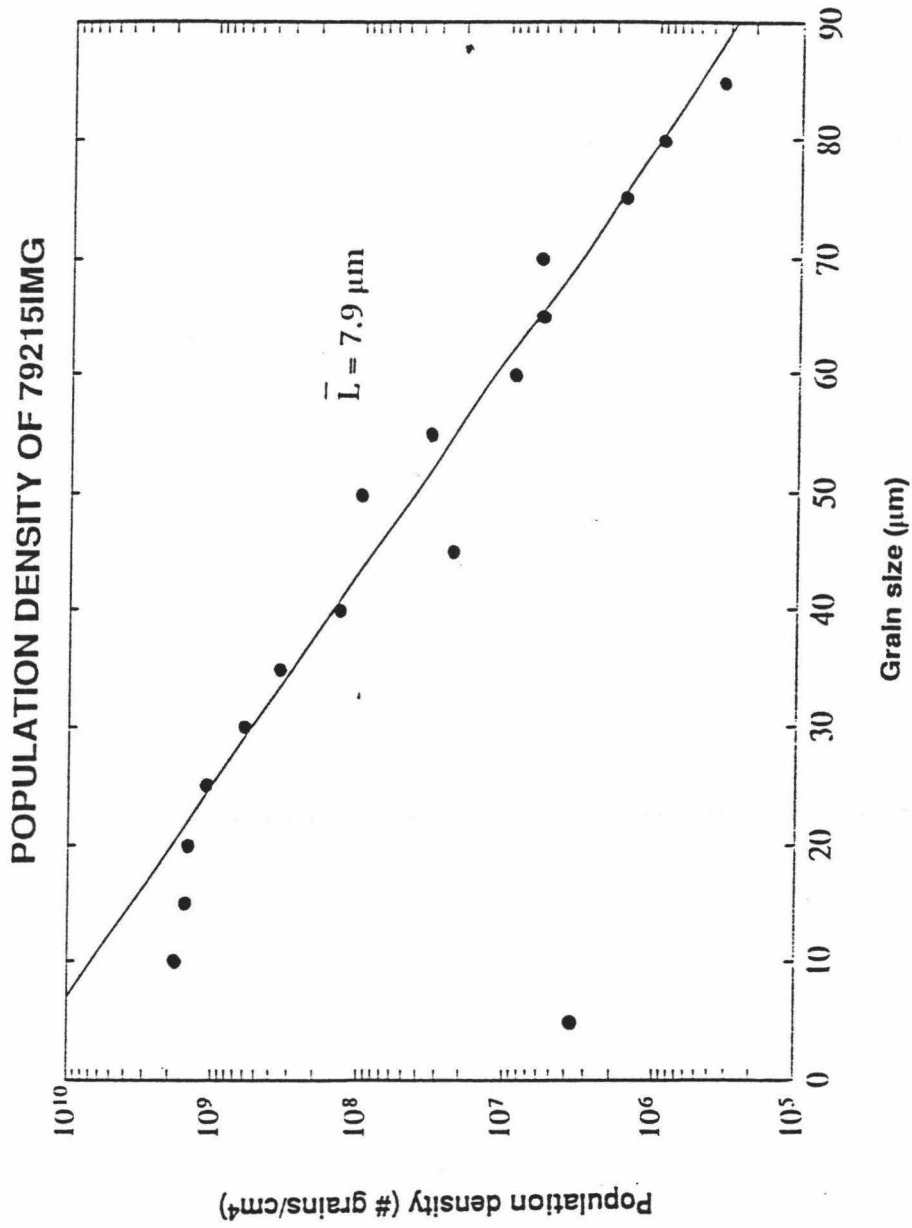
Ostwald ripening equation (Eq. 4). The diffusion coefficient for olivine (Misener, 1974) was used because the CSDs include olivine grains. Also, the diffusion coefficient for olivine is reasonably. well-determined and provides self-consistent results for chondrite metamorphism (Jones and Rubie, 1991; McCoy et al., 1991; G.J. Taylor and T. McCoy, unpublished results).

Table 5 gives the initial and final grain sizes, and cooling rates for 79215 and 67915 for the duration of metamorphism to 1000°C (there is no significant grain growth below this temperature). Initial temperatures use the 2-pyroxene temperatures obtained by the Kretz method. The grain growth program was run at a variety of cooling rates to find one which corresponded with the observed final grain size.

Table 5. Cooling Rates for Granoblastic Samples

Sample	Initial Temperature (°C)	Initial Grain Radius (μm)	Final Grain Radius (μm)	Cooling Rate (°C/yr)
67915	1068	3.93	11.58	0.65
79215man	1082	3.38	11.12	1.2
79215img	1082	3.95	10.57	1.4

The grain growth program also provides a way of computing the duration of metamorphism for the granoblastic rocks (Figures 14, 15, and 16). Assuming isothermal annealing at the initial temperatures given in Table 5, the time necessary for the amount of average grain growth is relatively short, $< 10^3$ years. So, the textures of these granoblastic rocks are not due to regional metamorphism, as previously thought by some, but of a more localized nature more akin to contact metamorphism.
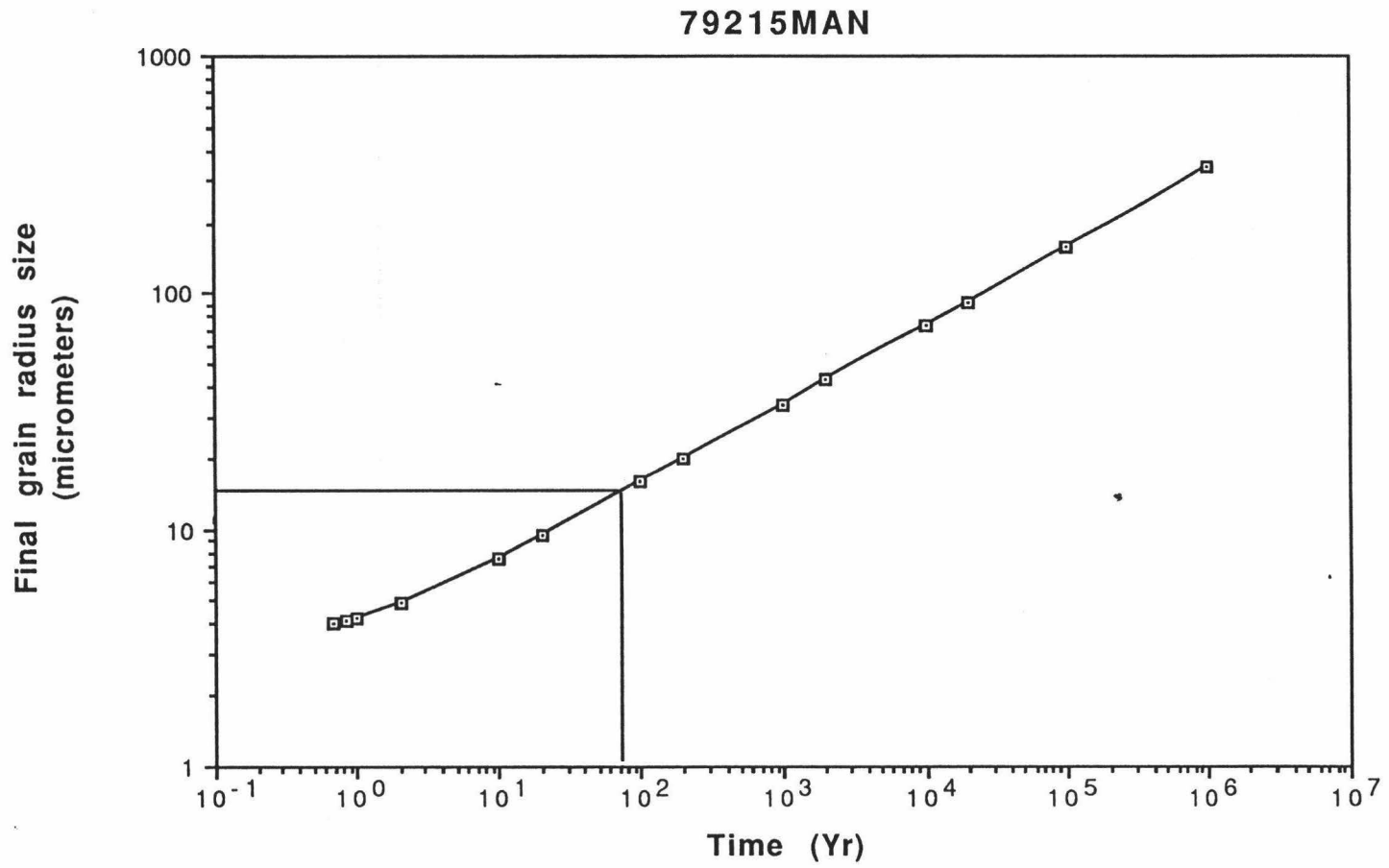
Figure 14. Duration of metamorphism for 79215man held at a peak equilibration temperature of 1082 degrees C. The final average grain size would reach 11 micrometers in about 75 years.

39
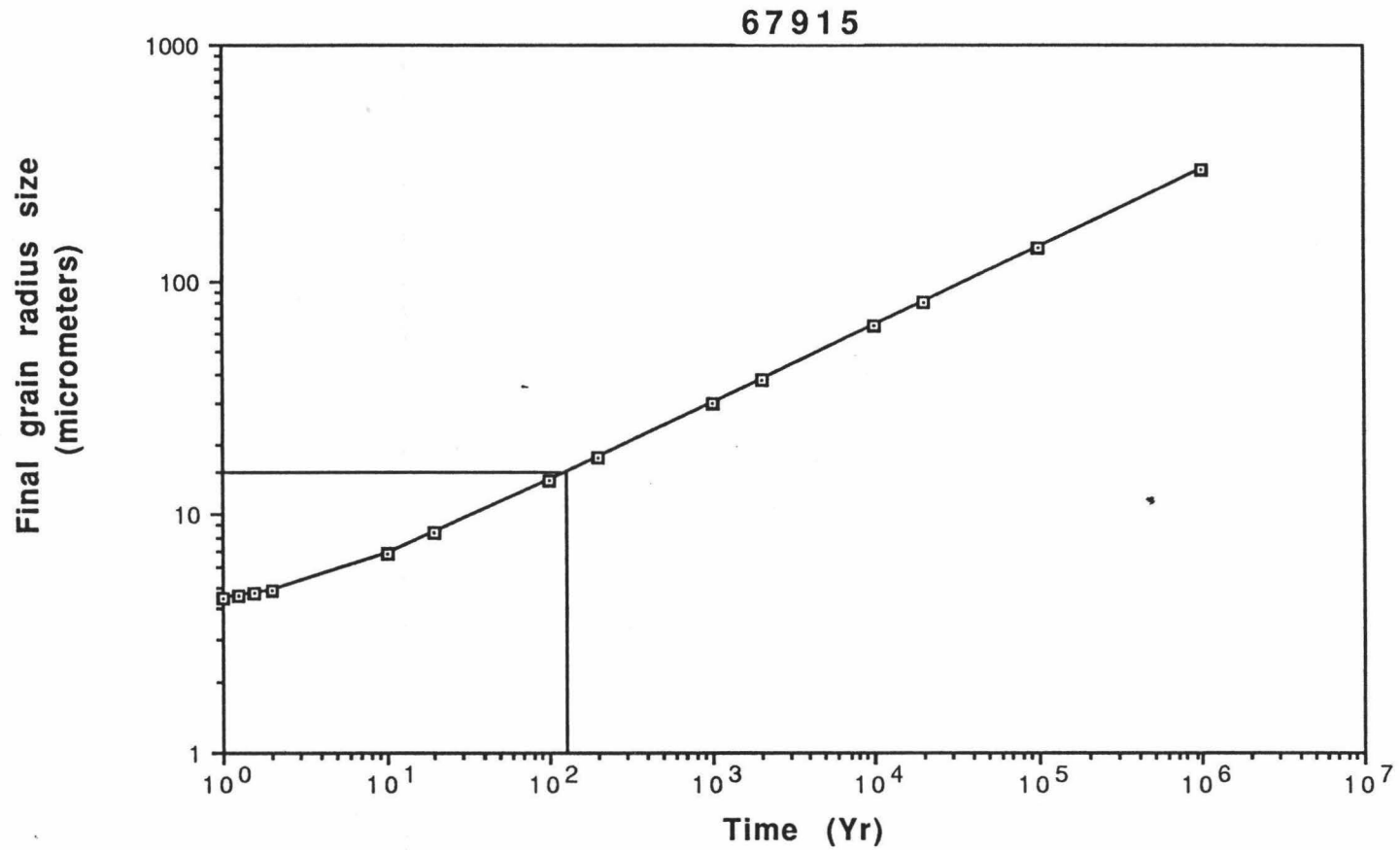
Figure 15. Duration of metamorphism for 67915 at a peak equilibration temperature of 1068 degrees C. Metamorphism lasted about 105 years to reach the observed final radius of 11.5 micrometers.
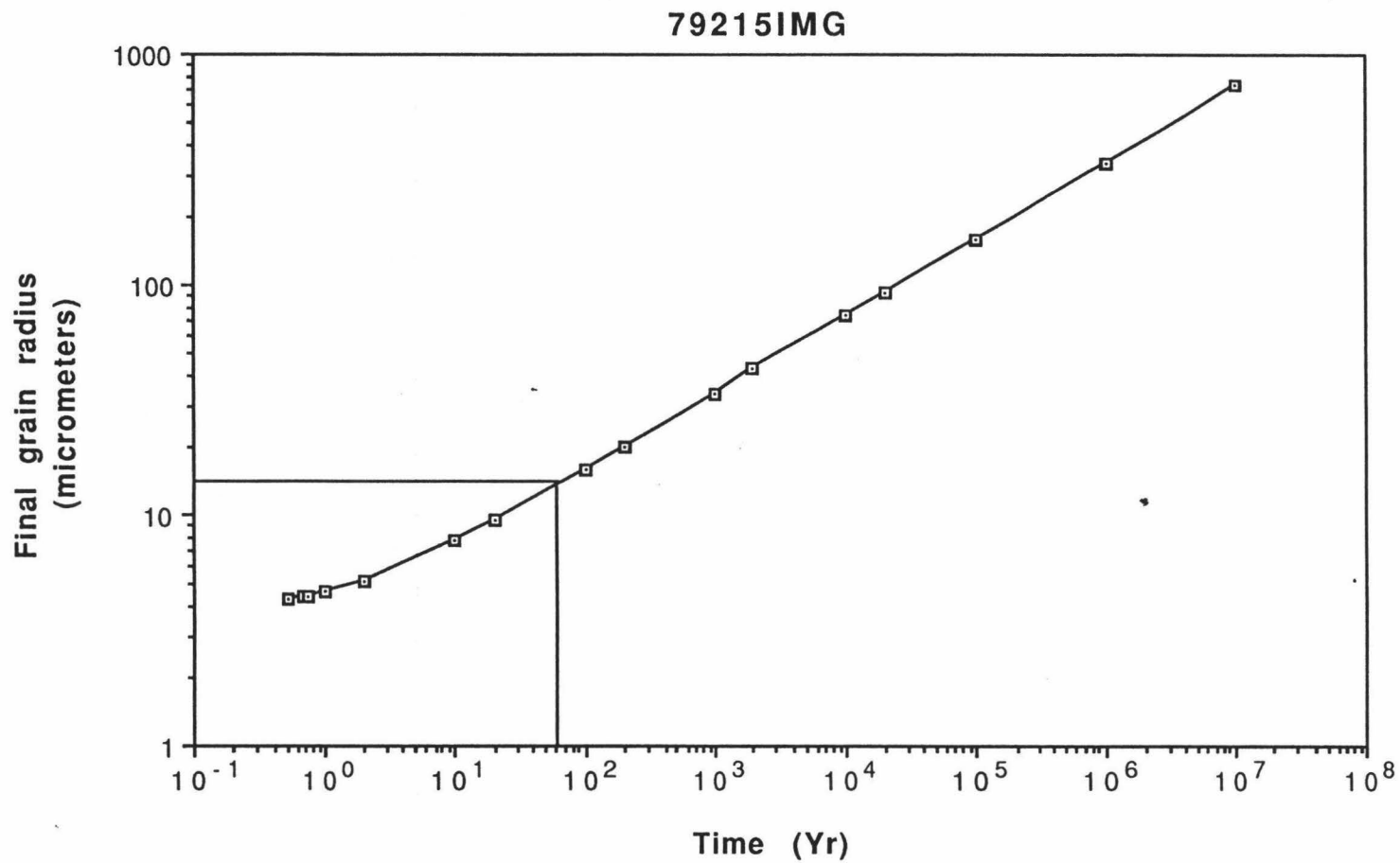
79215IMG

Figure 16. Duration of metamorphism for 79215img at a peak equilibrium temperature of 1082 degrees C. Metamorphism for the observed final radius lasted about 60 years.

Physical Setting

The equilibration temperatures and duration of cooling can be used to calculate the depths of burial to an order of magnitude accuracy. This can be done by assuming an extrusive slab of thickness $2a$ (in centimeters), cooling by radiation at the top and conduction at the bottom. In such a case, the final temperature T in degrees C, at time t in seconds, at a distance x from the midpoint of the slab is given by Jaeger (1968):

$$T/T_O = \phi\,(\xi,\, \tau) - \phi\,(2 - \xi,\, \tau) \tag{12}$$

where T_0 is the initial temperature,

$\phi\,(\xi,\, \tau) = 1/2\,\{erf\,[(\xi+1)/2\tau^{1/2}]\text{-}erf\,[(\xi\text{-}1)/2\tau^{1/2}]\}$, $\xi = x/a$, and $\tau = \kappa t/a^2$. κ is the thermal diffusivity of the rocks in the slab, and for most rocks is 0.01 cm^2/sec. The granoblastic samples were mostly likely buried in the center of a slab whose thicknesses are given for their cooling rates in Table 6.

Table 6. Burial depths for Granoblastic Samples

Sample	Initial T (°C)	τ	$2a$ (m)
67915	1068	0.1	361
79215man	1082	0.15	238
79215img	1082	0.15	220

For a more probable scenario, in which the breccias are buried under unconsolidated impact debris and melt, the thermal diffusivity will be lower. If an order of magnitude lower thermal diffusivity is assumed, this would result in a slab thinner by as much as a factor of $10^{1/2}$, or about 3, to the thicknesses given above.

Given the calculated cooling rates, duration of metamorphism, and burial depths for the most metamorphosed rocks, we can investigate the possible

42

physical settings for the impact breccias. The short cooling times and shallow burial of the rocks are inconsistent with long-term regional metamorphism. The rocks also could have been metamorphosed by intrusion of dikes, but their brecciated nature and compositional similarities to the poikilitic samples suggest that an impact crater setting is more likely. Two site in impact craters must be considered: under an ejecta blanket, and at the base of the impact crater. The shallow burial depth of the breccias allows both settings to be viable choices. The high temperatures (~1100°C) and the poikilitic textures seen in some of the impactites argue strongly for proximity to impact melts. In an impact crater, most of the melt is concentrated on and beneath the crater floor, and near the rim of the crater. Some of the melt is ejected, but can a sufficient mass of melt be ejected to provide the heating required to metamorphose the breccias? Studies of terrestrial craters such as the Ries in Germany (Miller and Wagner, 1979), suggest that this is unlikely, though the issue is still being debated. If only a minor amount of melt is emplaced in an ejecta blanket, it would be quickly quenched by the cold clasts and surrounding rock. Hence, the base of the impact crater, underneath a layer of impact melt breccia, is the most likely physical setting for the origin of the granulitic impact breccias (Figure 17). The granoblastic rocks underwent solid-state coarsening, and the poikilitic I group rocks were produced by impact melting, thus accounting for their igneous textures.

The setting for the poikilitic II rocks remains enigmatic. The mineralogy is the same for both poikilitic types, but the poikilitic I rocks have euhedral, medium-sized poikocrysts, while the poikilitic II rocks have tiny, rounded inclusions. Impact melting is the most likely origin for the poikilitic I rocks, but another possibility exists for the poikilitic II group. Starting with a previously crushed up matrix, an impact could cause the rock to heat to a critical

43
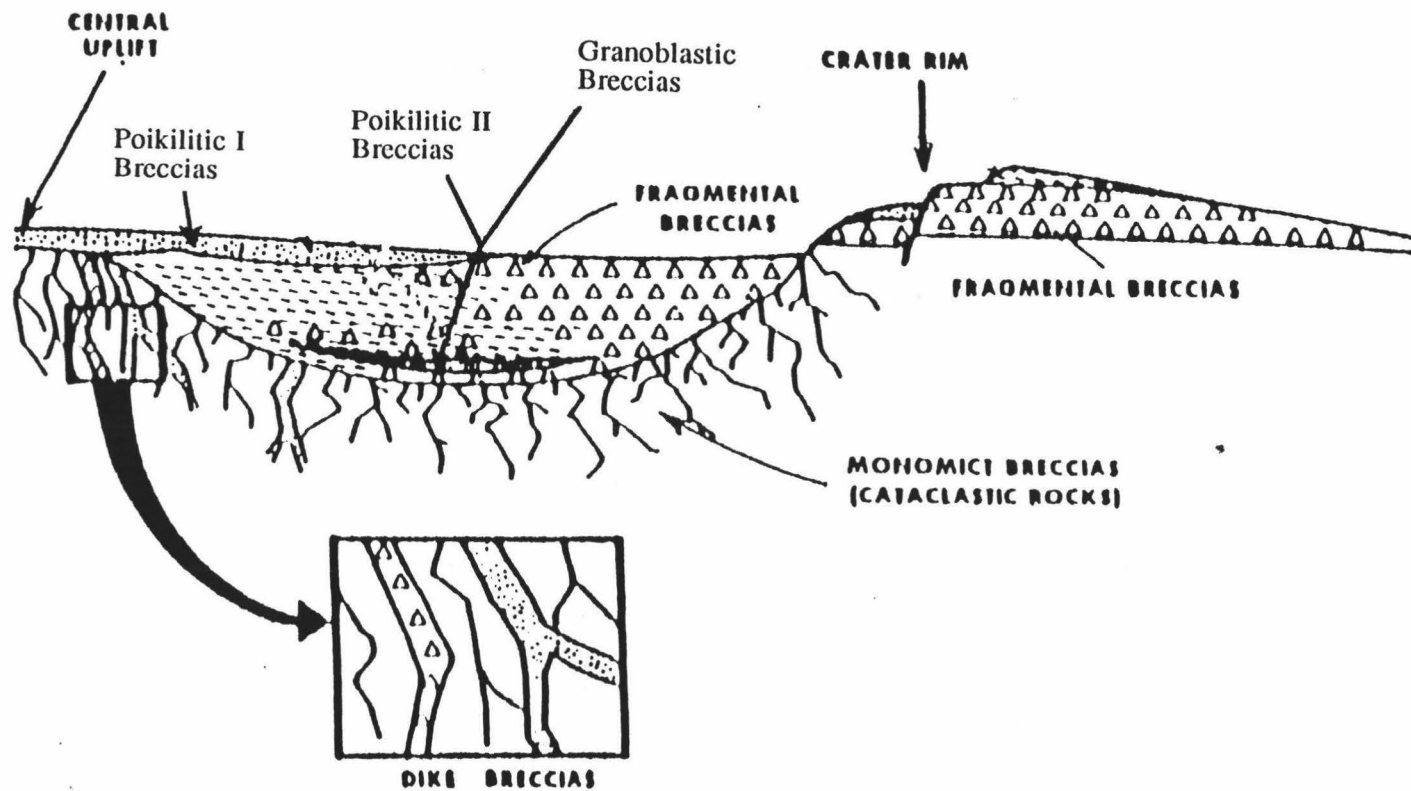
Figure 17. Physical setting of impact breccias in a medium-sized impact crater (modified after Stöffler, 1981).

Within the figure:

CENTRAL UPLIFT

Granoblastic Breccias

CRATER RIM

Poikilitic I Breccias

Poikilitic II Breccias

FRAGMENTAL BRECCIAS

FRAGMENTAL BRECCIAS

MONOMICT BRECCIAS (CATACLASTIC ROCKS)

DIKE BRECCIAS

44

temperature, near 1100°C. Ostwald ripening takes place, where a chain of pyroxene crystals merge to form one big crystal (see fig. 19 in Shaw, 1989). This irregularly shaped crystal forms around plagioclase grains, which themselves have become rounded due to heating. The poikilitic II textures occur in some of the granoblastic samples, suggesting a link. Thus, slight textural variations may have led to the production of poikilitic II rocks in some cases and granoblastic in others. A combination of the pre-existing textures and slightly higher temperatures may have resulted in liquid-phase sintering for the poikilitic II rocks.

CHAPTER 5
IMPLICATIONS

The numerous clasts and breccia-within-breccia textures that are often seen in these rocks suggest that the melting and metamorphism episodes described above may be common occurrences. Every impact event of substantial size would produce impact melts (poikilitic I rocks) and thermally metamorphosed (poikilitic II and granoblastic) rocks. Some of these rocks were probably affected by several impacts, with the observed textures displaying the latest impact event. The size of the impact event is constrained to be smaller than basin-sized events because there is no KREEPy (potassium and rare earth elements) component and no LKFM (low-K Fra Mauro basalts) in the impact breccias. These two components are associated with the lunar basins. The impact events must, however, be large enough to produce substantial amounts of melt. The minimum crater size range to produce a large enough melt sheet is 5-20 km. Probably, craters within the 10-100 km range were responsible for production of most of the granulitic impactites; there are numerous craters of those sizes on the Moon.

Chemical groupings indicate at least four groups based on Fe/Mg ratios (Lindstrom and Lindstrom, 1986): strongly ferroan, moderately ferroan, strongly magnesian, and moderately magnesian. Due to the poor sampling of the Moon, there may be other rock types, or a continuum among the four groups mentioned above. If such is the case, then the number of targets is quite extensive. This is consistent with the early cratering history of the Moon.

CHAPTER 6
CONCLUSIONS

My investigations into the rocks of the granulitic impactite suite have resulted in the following conclusions.

1. There are three different types of impactite breccias: poikilitic I, poikilitic II, and granoblastic breccias.

2. The three types of impactites have similar equilibration temperatures, as well as common compositions. These factors suggest that the groups are related to each other.

3. CSD studies reveal that Ostwald ripening took place, and solid-state grain growth calculations have yielded a short duration ($< 10^3$ years) of metamorphism.

4. The granoblastic rocks were buried at a relatively shallow level (< 500 m). The poikilitic I rocks were melted by the impact. The poikilitic II rocks were metamorphosed and may have undergone liquid-phase sintering, rather than just solid-state metamorphism like the granoblastic rocks.

APPENDIX A
ELECTRON MICROPROBE SETUPS

Below are the setups used for pyroxene and olivine analyses on the
electron microprobe, including detection limits and analytical uncertainties.

Table 7. Pyroxene

Element	Standard	Crystal	Time (seconds)	Detection Limit (wt. %)	Analytical Uncertainty (%) Relative
SiO_2	Kakanui Augite	TAP	30	0.021	0.053
MgO	Kakanui Augite	TAP	30	0.018	0.071
Al_2O_3	Kakanui Augite	TAP	60	0.013	0.008
CaO	Kakanui Augite	PET	30	0.022	0.116
FeO	Hypersthene	LIF	30	0.039	0.074
MnO	Verma Garnet	LIF	60	0.027	0.010
TiO_2	Sphene Glass	PET	60	0.016	0.007
Cr_2O_3	Chromite	LIF	60	0.025	0.010
Na_2O	Jadite	TAP	40	0.020	0.019

Table 8. Olivine

Element	Standard	Crystal	Time (seconds)	Detection Limit (wt. %)	Analytical Uncertainty (%) Relative
SiO_2	San Carlos Olivine	TAP	30	0.023	0.065
CaO	Kakanui Augite	PET	70	0.014	0.003
FeO	Magnetite	LIF	30	0.051	0.069
MgO	San Carlos Olivine	TAP	30	0.019	0.101
MnO	Verma Garnet	LIF	60	0.027	0.009

APPENDIX B
MICROPROBE ANALYSES

Microprobe analyses of the lunar samples are provided in the following pages.

Table 9. Microprobe data of 15418,98									
Pyroxene		Date	11/10/92						
		Time	22:11						
Grain #	SiO2	TiO2	Al2O3	Cr2O3	FeO	MgO	CaO	MnO	Na2O	Total
1a	52.23	0.87	2.00	0.38	10.24	14.43	19.62	0.19	0.05	99.99
1b	52.27	0.82	1.60	0.38	9.52	14.69	20.42	0.25	0.06	99.99
1c	51.70	0.58	2.03	0.47	13.35	17.38	13.91	0.27	0.03	99.72
1d	52.97	0.30	0.67	0.19	21.13	22.24	1.44	0.34	0.00	99.28
1e	52.90	0.32	0.66	0.17	19.49	21.50	4.09	0.38	0.02	99.52
2a	51.34	1.23	1.95	0.42	10.20	14.33	19.65	0.22	0.08	99.43
2b	51.30	0.80	1.63	0.54	11.30	15.76	18.96	0.26	0.04	100.60
2c	51.69	0.82	2.05	0.41	9.68	14.69	20.51	0.21	0.06	100.12
2d	53.75	0.31	0.68	0.23	18.80	23.13	2.69	0.32	0.03	99.94
2e	52.70	0.62	1.46	0.27	12.52	15.94	16.02	0.25	0.03	99.81
3a	51.76	0.87	1.93	0.46	9.13	14.68	20.64	0.21	0.06	99.74
3b	51.46	1.15	1.89	0.40	10.54	14.30	20.04	0.18	0.04	100.01
3c	52.07	0.60	1.27	0.29	9.33	15.09	20.12	0.20	0.05	99.02
3d	52.99	0.34	0.89	0.22	20.11	22.45	2.23	0.38	0.03	99.64
4a	51.77	0.84	1.82	0.50	8.94	14.54	20.80	0.23	0.06	99.51
4b	51.57	0.83	1.75	0.41	8.99	14.92	20.12	0.22	0.07	98.88
4c	52.64	0.63	1.45	0.30	10.34	14.93	19.00	0.23	0.05	99.57
5a	51.67	1.26	1.81	0.44	10.25	14.68	19.85	0.20	0.07	100.23
5b	51.78	1.25	1.80	0.42	9.98	14.67	20.17	0.22	0.05	100.78
5c	53.19	0.34	0.56	0.26	19.52	22.50	2.60	0.36	0.03	99.35

Table 9. (Continued) Microprobe data of 15418,98										
Olivine		Date	4/8/93							
		Time	18:30							
Grain #	SiO2	FeO	MgO	CaO	MnO	Total				
10 (1)	34.95	38.13	25.43	0.05	0.37	98.94				
2	35.14	38.49	25.45	0.06	0.40	99.54				
8(8)	35.20	38.64	25.52	0.07	0.38	99.81				
9	35.64	37.70	25.98	0.12	0.37	99.82				
7(11)	35.07	37.96	25.30	0.11	0.39	98.83				
6 (13)	35.17	37.70	25.50	0.20	0.40	98.97				
14	35.10	38.66	25.09	0.27	0.38	99.51				

51

Table 10. Microprobe Data of Olivine Profile in 15418,98						
Grain #8			**Date**	7/12/93		
Analyses space 2 micrometers apart			**Time**	12:31:24		
Point #	**SiO2**	**FeO**	**MgO**	**CaO**	**MnO**	**Total**
2	35.42	37.55	26.80	0.14	0.39	100.30
3	35.28	38.25	26.44	0.16	0.41	100.53
4	35.27	37.94	26.78	0.17	0.38	100.53
5	35.32	38.02	26.79	0.14	0.43	100.70
6	35.71	36.31	27.51	0.51	0.41	100.46
7	35.46	37.16	27.11	0.42	0.40	100.56
8	35.40	38.07	26.59	0.18	0.41	100.65
9	35.50	38.11	26.73	0.08	0.41	100.83
10	35.28	38.69	26.55	0.07	0.39	100.98
11	35.47	38.14	26.54	0.07	0.43	100.65
12	35.29	38.59	26.50	0.08	0.40	100.86
13	35.43	38.63	26.37	0.12	0.42	100.98
14	35.26	38.79	26.39	0.08	0.41	100.92
15	35.34	38.37	26.64	0.08	0.40	100.82
16	35.42	38.39	26.51	0.08	0.41	100.81
17	35.37	38.52	26.62	0.08	0.41	101.00
18	35.27	38.47	26.70	0.12	0.39	100.95
19	35.93	37.09	26.16	0.66	0.39	100.23
20	35.78	37.17	26.47	0.65	0.39	100.46
21	35.59	37.91	26.01	0.62	0.40	100.52
22	35.34	38.11	26.95	0.18	0.38	100.96
23	35.45	37.94	26.84	0.13	0.40	100.77
24	35.52	37.76	26.81	0.17	0.40	100.65
25	35.32	37.36	27.18	0.21	0.39	100.46

52

Table 11. Microprobe data of 60035,17										
Pyroxene		**Date**	11/6/92							
		Time	14:01							
Grain #	**SiO2**	**TiO2**	**Al2O3**	**Cr2O3**	**FeO**	**MgO**	**CaO**	**MnO**	**Na2O**	**Total**
Aa	51.66	2.04	3.01	0.94	5.56	17.62	19.22	0.12	0.10	100.28
Ab	51.09	2.43	3.37	0.98	5.05	16.96	20.42	0.13	0.10	100.52
Ac	55.64	0.97	1.34	0.52	11.22	29.57	2.06	0.18	0.00	101.49
Olivine		**Date**	5/1/93							
Grain #	**SiO2**	**FeO**	**MgO**	**CaO**	**MnO**	**Total**				
z (13)	38.75	18.24	43.39	0.09	0.26	100.72				
14	39.35	17.97	42.83	0.06	0.23	100.44				
15	39.67	17.67	42.22	0.09	0.19	99.83				
16	39.44	17.86	42.11	0.10	0.23	99.75				
17	39.78	17.89	42.36	0.09	0.24	100.36				
y (18)	39.87	16.53	44.14	0.09	0.23	100.87				
19	39.97	16.65	43.52	0.07	0.19	100.40				
20	40.72	16.70	42.87	0.07	0.21	100.57				
1 (21)	39.96	15.72	44.71	0.07	0.23	100.70				
23	40.32	15.56	44.08	0.05	0.18	100.19				

Table 12. Microprobe data of 67215,5										
Pyroxene Random zoning checks		Date	5/2/93							
Grain #	SiO2	TiO2	Al2O3	Cr2O3	FeO	MgO	CaO	MnO	Na2O	Total
1 (4)	52.24	0.47	0.52	0.16	24.72	19.40	2.71	0.41	0.00	100.63
5	52.47	0.49	0.48	0.16	25.09	20.08	1.30	0.40	0.00	100.48
6	51.81	0.34	0.49	0.12	24.95	19.83	1.60	0.43	0.00	99.56
2 (7)	53.09	0.48	0.61	0.19	21.81	18.44	5.27	0.38	0.00	100.26
8	52.72	0.57	0.48	0.22	23.06	20.04	3.06	0.39	0.00	100.53
9	52.83	0.35	0.63	0.18	23.38	20.04	3.18	0.40	0.00	100.99
2 actual (10)	52.13	0.47	0.52	0.15	23.78	19.92	3.71	0.45	0.00	101.12
11	52.42	0.49	0.54	0.17	23.13	19.48	3.54	0.43	0.00	100.20
12	52.22	0.38	0.59	0.16	23.45	20.41	2.63	0.43	0.00	100.27

Table 13. Microprobe Data of 67415,113										
Pyroxene		Date	11/11/92							
		Time	16:12							
Grain #	SiO2	TiO2	Al2O3	Cr2O3	FeO	MgO	CaO	MnO	Na2O	Total
11	51.73	1.95	2.30	0.67	6.21	16.94	20.34	0.16	0.19	100.48
10	53.48	0.94	1.12	0.43	13.69	28.16	1.77	0.27	0.03	99.89
26	53.59	0.75	0.68	0.32	16.41	26.18	1.71	0.28	0.02	99.93
25a	50.45	2.27	2.67	0.66	6.99	16.20	20.01	0.11	0.22	99.58
25b	51.77	2.14	2.46	0.63	7.33	16.72	19.37	0.21	0.18	100.80
34a	52.25	1.37	2.22	0.76	6.27	16.92	19.93	0.17	0.19	99.98
35b	52.93	1.02	1.77	0.47	11.83	22.92	9.64	0.22	0.10	100.49
35a	52.22	1.60	2.14	0.75	6.38	16.96	20.16	0.17	0.20	100.58
c=center		Date	11/21/92							
e=edge										
Grain #	SiO2	TiO2	Al2O3	Cr2O3	FeO	MgO	CaO	MnO	Na2O	Total
Ac	52.72	1.85	1.85	0.48	13.60	26.66	2.29	0.26	0.02	99.73
Ae	52.62	1.72	1.80	0.49	13.92	26.87	2.11	0.26	0.01	99.81
Bc	53.35	1.21	1.11	0.40	14.63	26.68	2.18	0.26	0.02	99.84
Be	53.09	1.67	1.60	0.47	14.84	26.19	2.37	0.25	0.00	100.49
Cc	54.10	1.04	0.96	0.41	13.22	28.12	1.75	0.25	0.00	99.84
Ce	53.39	1.52	1.65	0.54	12.95	27.48	1.87	0.25	0.00	99.64
Dc	53.47	1.73	1.68	0.50	12.72	27.65	2.38	0.23	0.01	100.37
De	53.99	1.67	1.59	0.61	12.72	27.55	2.12	0.24	0.01	100.49

Table 13. (Continued) Microprobe Data of 67415,113										
Olivine		Date	5/1/93							
		Time	17:14							
Grain #	SiO2	FeO	MgO	CaO	MnO	Total				
E (1)	38.47	22.68	39.07	0.43	0.22	100.87				
2	38.24	23.27	38.36	0.16	0.21	100.25				
3	38.84	22.67	38.25	0.22	0.25	100.22				

Table 14. Microprobe Data of 67915,221										
Pyroxene		Date	10/11/92							
		Time	20:34							
Grain #	SiO2	TiO2	Al2O3	Cr2O3	FeO	MgO	CaO	MnO	Na2O	Total
4	50.08	1.12	11.69	0.43	4.39	12.36	20.58	0.10	0.28	101.03
3	54.55	0.70	1.30	0.42	13.85	27.22	1.71	0.24	0.02	100.02
		Date	11/22/92							
Grain #	SiO2	TiO2	Al2O3	Cr2O3	FeO	MgO	CaO	MnO	Na2O	Total
1	51.17	1.50	2.20	0.93	6.24	16.40	20.79	0.16	0.12	99.51
2	54.63	0.62	0.93	0.49	14.16	27.86	1.88	0.25	0.02	100.90
3	53.95	0.73	1.15	0.55	14.25	27.81	1.83	0.24	0.03	100.53
4	51.28	1.68	2.52	0.94	6.52	16.75	20.51	0.14	0.12	100.47
5;1a	52.79	0.70	3.41	0.53	12.21	26.74	2.35	0.25	0.04	99.03
5;1b	51.99	0.76	1.55	0.58	13.70	30.40	1.70	0.26	0.04	100.97
6a	50.16	1.57	1.71	0.46	12.01	13.50	19.50	0.23	0.17	99.30
6b	55.67	1.63	1.72	0.48	12.02	13.53	19.57	0.24	0.19	100.06
		Date	11/21/92							
Grain #	SiO2	TiO2	Al2O3	Cr2O3	FeO	MgO	CaO	MnO	Na2O	Total
Gc	51.02	1.50	1.57	0.31	12.04	13.75	19.18	0.24	0.17	99.79
Ge	51.56	1.50	1.51	0.34	12.50	13.64	19.60	0.29	0.16	101.09

57

Table 14. (Continued) Microprobe Data of 67915,221										
Olivine		Date	5/1/93							
Grain #	SiO2	FeO	MgO	CaO	MnO	Total				
E (4)	38.60	23.60	38.10	0.06	0.26	100.62				
5	38.23	23.27	38.15	0.05	0.25	99.95				
J (7)	38.38	24.79	37.28	0.06	0.31	100.80				
8	38.19	24.70	37.15	0.06	0.24	100.34				
9	38.23	24.38	37.08	0.07	0.27	100.02				
B (10)	39.57	18.60	41.67	0.07	0.19	100.11				
11	39.24	18.49	42.06	0.06	0.25	100.10				
12	39.29	18.71	41.85	0.10	0.20	100.15				

58

Table 15. Microprobe Data of 67955,52									
Pryoxene		date	11/7/92						
Grain #	**SiO2**	**TiO2**	**Al2O3**	**Cr2O3**	**FeO**	**MgO**	**CaO**	**MnO**	**Na2O**
Aa	51.41	1.99	3.01	0.86	5.51	17.09	20.68	0.12	0.16
Ab	50.75	2.29	3.27	0.97	5.69	17.29	20.03	0.15	0.18
Acc	51.20	1.74	2.88	0.65	5.15	17.27	20.83	0.16	0.14
Olivine		Date	11/14/92						
		Time	14:28						
Grain #	**SiO2**	**FeO**	**MgO**	**CaO**	**MnO**	**Total**			
1c	38.51	21.42	40.64	0.04	0.23	100.84			
1e	38.30	21.29	40.85	0.06	0.23	100.72			
2c	36.44	20.76	42.68	0.06	0.20	100.14			
2e	38.47	21.42	40.82	0.05	0.22	100.99			
4c	38.77	21.22	40.68	0.06	0.23	100.96			
4e	38.18	21.41	40.98	0.07	0.21	100.85			
5c	37.78	21.49	40.75	0.05	0.23	100.30			
9e	38.54	20.76	41.24	0.03	0.21	100.79			
6e	38.12	21.34	41.16	0.09	0.24	100.95			
10e	38.73	20.66	41.18	0.09	0.22	100.89			

Table 15. (Continued) Microprobe Data of 67955,52									
Olivine		Date	4/8/93						
Grain #	SiO2	FeO	MgO	CaO	MnO	Total			
2	38.85	21.64	39.31	0.08	0.22	100.09			
3	38.78	21.15	40.57	0.07	0.24	100.81			
16 (16)	38.86	20.17	41.00	0.10	0.20	100.33			
17	38.92	20.34	41.20	0.04	0.24	100.73			
18	38.85	19.69	40.66	0.08	0.21	99.49			
15 (19)	38.54	21.05	40.32	0.08	0.23	100.22			
20	38.66	21.12	40.90	0.08	0.22	100.97			
21	38.77	20.96	40.10	0.10	0.23	100.16			
14 (22)	38.90	20.84	39.77	0.07	0.21	99.79			
23	38.90	20.71	40.77	0.06	0.24	100.67			
24	38.77	20.41	40.56	0.07	0.22	100.03			
13 (26)	38.74	20.79	39.67	0.05	0.24	99.49			
27	39.01	21.10	39.99	0.07	0.23	100.40			

Table 16. Microprobe data of 72559,10									
Pyroxene		**Date**	10/22/92						
Grain #	**SiO2**	**TiO2**	**Al2O3**	**Cr2O3**	**FeO**	**MgO**	**CaO**	**MnO**	**Na2O**	**Total**
1;6a	54.88	0.95	1.49	0.75	10.64	29.64	1.71	0.22	0.03	100.30
1;6b	54.46	0.96	1.55	0.71	10.63	29.92	1.76	0.20	0.03	100.21
1;6c	51.60	1.87	2.75	1.11	4.68	17.05	21.33	0.11	0.08	100.58
1;8a	51.22	1.91	2.73	0.98	4.58	17.08	21.08	0.15	0.12	99.84
1;8b	54.76	0.83	1.47	0.65	10.62	30.04	1.68	0.24	0.03	100.31
2;9	54.66	0.87	1.48	0.69	10.42	29.93	1.76	0.20	0.04	100.05
Pyroxene		**Date**	11/21/92						
		Time	14:50						
Grain #	**SiO2**	**TiO2**	**Al2O3**	**Cr2O3**	**FeO**	**MgO**	**CaO**	**MnO**	**Na2O**	**Total**
3;Ec a	54.39	1.18	1.80	0.45	10.77	29.79	1.37	0.23	0.00	99.97
3;Ee b	55.39	0.71	1.05	0.27	10.98	30.66	1.19	0.18	0.00	100.43
3;Ee c	54.96	0.78	1.17	0.32	10.89	30.46	1.24	0.23	0.00	100.04

Table 16. (Continued) Microprobe data of 72559,10									
Olivine	c=center	Date	11/14/92						
	c=edge	Time	19:06						
Point #	SiO2	FeO	MgO	CaO	MnO	Total			
1; Ac	38.88	18.24	42.01	0.06	0.21	99.39			
1; Ae	38.76	18.09	42.11	0.09	0.21	99.24			
1; Cc	38.83	18.67	42.21	0.05	0.20	99.96			
1; Ce	38.60	18.17	42.12	0.09	0.18	99.17			
2; Bc	38.84	18.32	42.31	0.07	0.21	99.75			
2; Be	38.84	17.83	42.22	0.11	0.23	99.22			
3; Ac	38.86	18.44	42.14	0.06	0.20	99.69			
3; Ae	38.73	18.40	42.08	0.06	0.21	99.47			
3;Dc	38.88	18.07	42.60	0.06	0.19	99.81			
3; De	39.12	17.90	42.28	0.07	0.20	99.57			

62

Table 17. Microprobe data of 73215,336										
Pyroxene	c=center	**Date**	7/13/93							
	e=edge	**Time**	10:00							
Grain #	**SiO2**	**TiO2**	**Al2O3**	**Cr2O3**	**FeO**	**MgO**	**CaO**	**MnO**	**Na2O**	**Total**
6 (cpx)-pt. 4	51.15	1.62	2.56	0.75	6.23	16.92	19.89	0.11	0.08	99.31
7 (opx)-pt. 3	54.24	0.88	1.61	0.53	12.21	28.91	1.93	0.19	0.01	100.52
8 (cpx)	52.30	1.37	2.26	0.68	5.62	17.70	19.88	0.11	0.07	99.99
9 (cpx)-pt. 8	51.63	1.49	2.52	0.70	6.39	17.77	18.79	0.11	0.07	99.47
10 (cpx)	52.47	1.29	2.08	0.64	6.50	19.78	16.29	0.14	0.07	99.26
11 (opx)-pt. 6	54.35	0.71	1.22	0.48	11.63	28.33	2.95	0.19	0.01	99.87
12 (cpx)	51.51	1.49	2.50	0.75	5.57	17.09	20.21	0.12	0.08	99.33
13 (opx)-pt.10	54.69	0.73	1.25	0.47	12.20	29.27	1.67	0.17	0.00	100.44
14 (cpx)	51.55	1.44	2.31	0.72	5.82	17.24	20.01	0.12	0.09	99.29
15 (opx)	54.43	0.89	0.99	0.37	12.50	25.75	5.42	0.19	0.02	100.56
16 (cpx)	51.64	1.45	2.36	0.69	5.71	17.14	20.19	0.12	0.09	99.38

63

Table 18. Microprobe data of 73215,339									
Pyroxene	c=center	Date	7/13/93						
	e=edge	Time	10:00						
Grain #	SiO2	TiO2	Al2O3	Cr2O3	FeO	MgO	CaO	MnO	Na2O	Total
1	50.27	1.18	9.12	0.58	4.50	13.74	20.33	0.10	0.16	99.98
2	54.45	0.57	1.04	0.39	11.98	28.73	2.52	0.18	0.01	99.88
3	51.50	1.42	2.53	0.71	6.18	17.18	19.44	0.15	0.08	99.18
4 -same as 3	51.01	1.80	2.73	0.79	6.36	17.25	19.01	0.12	0.10	99.17
5	54.35	0.59	1.14	0.40	12.12	28.77	1.70	0.19	0.01	99.26

64

Table 19. Microprobe data of 76230,11									
Pyroxene		Date	11/10/92						
		Time	0:45						
Grain #	SiO2	TiO2	Al2O3	Cr2O3	FeO	MgO	CaO	MnO	Na2O	Total
1a-3	51.28	1.72	2.45	0.77	7.26	16.53	19.09	0.15	0.15	99.40
1b	54.56	0.98	1.49	0.52	14.45	26.12	2.17	0.25	0.01	100.56
2	51.28	1.97	2.74	0.75	6.92	16.34	19.85	0.18	0.10	100.13
3	51.50	2.03	2.82	0.78	7.10	17.04	18.89	0.15	0.14	100.44
4	53.75	0.74	1.11	0.41	14.27	26.69	1.80	0.28	0.03	99.08
8	51.32	1.82	2.63	0.85	7.08	16.44	19.58	0.15	0.15	100.02
9	53.03	0.72	0.91	0.42	15.82	26.00	3.26	0.31	0.05	100.52

Table 19. (Continued) Microprobe data of 76230,11										
Olivine		Date	4/23/93							
edge-center-edge		Time	14:23							
Grain #	SiO2	FeO	MgO	CaO	MnO	Total				
1 (6)	37.85	23.79	37.51	0.14	0.24	99.53				
2	37.83	23.99	37.33	0.13	0.25	99.53				
3	38.42	23.95	37.78	0.10	0.22	100.47				
4 (5)	38.37	23.65	37.46	0.12	0.22	99.81				
5	38.01	23.54	37.47	0.16	0.25	99.42				
6										
7 (4)	38.02	23.89	37.46	0.17	0.20	99.74				
8	37.79	24.47	37.24	0.16	0.25	99.91				
9	37.97	24.21	37.39	0.18	0.25	100.00				
10 (3)	38.18	23.29	38.17	0.11	0.23	99.98				
11	38.37	23.58	38.29	0.10	0.24	100.57				
12	38.41	23.40	38.33	0.14	0.23	100.51				
13	38.32	23.37	38.32	0.08	0.23	100.32				
14	38.05	23.13	38.46	0.10	0.24	99.98				
15 (2)	37.52	23.37	37.80	0.11	0.22	99.03				
16	38.15	23.75	38.11	0.09	0.24	100.34				
18	38.16	23.79	37.83	0.17	0.23	100.16				
19*	38.39	24.09	37.66	0.14	0.24	100.51				
20* same	38.19	23.70	37.56	0.16	0.24	99.85				
21	38.55	23.53	37.59	0.21	0.22	100.09				

Table 20. Microprobe data of 76235,17									
Pyroxene		Date	11/7/92						
		Time	17:04						
Grain #	SiO2	TiO2	Al2O3	Cr2O3	FeO	MgO	CaO	MnO	Na2O	Total
Aa	51.81	1.83	2.48	0.73	7.01	16.58	19.42	0.15	0.11	100.10
Ab	52.58	1.50	2.03	0.64	6.97	16.81	19.92	0.16	0.10	100.70
Ac	50.86	1.89	2.62	0.64	7.33	16.47	19.26	0.17	0.09	99.32
Ad	53.90	0.67	0.80	0.36	15.67	24.88	3.85	0.28	0.03	100.44
Ba	52.03	1.87	2.63	0.76	7.83	16.13	19.29	0.17	0.16	100.87
Bb	54.63	0.76	1.43	0.36	15.04	24.24	4.17	0.29	0.05	100.98
Ca	51.50	2.06	2.64	0.65	7.54	16.40	19.10	0.16	0.12	100.17
Cb	52.45	1.44	2.03	0.60	10.57	19.79	13.06	0.19	0.07	100.19
Cc	54.17	1.01	1.35	0.49	14.82	26.24	2.11	0.25	0.02	100.46
Cd	54.20	1.04	1.36	0.46	14.21	26.40	2.37	0.27	0.02	100.32
Ce	54.16	0.93	1.24	0.44	14.91	26.31	2.00	0.27	0.09	100.27

67

Table 21. Microprobe data of 77017,160									
Pyroxene		**Date**	10/9/92						
Point #	**SiO2**	**TiO2**	**Al2O3**	**Cr2O3**	**FeO**	**MgO**	**CaO**	**MnO**	**Na20**	**Total**
8a	51.11	1.47	3.15	0.58	10.19	15.89	17.62	0.17	0.09	100.27
8b	52.84	0.78	1.16	0.42	17.02	22.46	5.63	0.30	0.04	100.65
8c	52.79	0.89	1.55	0.55	14.63	21.03	8.28	0.23	0.07	100.03

Table 22. Microprobe data of 77017,161									
Pyroxene		**Date**	10/9/92						
Grain #	**SiO2**	**TiO2**	**Al2O3**	**Cr2O3**	**FeO**	**MgO**	**CaO**	**MnO**	**Na2O**	**Total**
2c	51.06	1.68	2.22	0.52	10.26	15.29	18.28	0.22	0.13	99.66
2o	53.15	0.47	0.55	0.25	19.94	22.80	2.30	0.33	0.03	99.82
4o	53.29	0.70	0.80	0.36	17.37	23.15	3.88	0.30	0.03	99.86
4c	51.41	1.45	2.36	0.75	8.91	16.10	18.74	0.18	0.09	99.99
4a2-c	51.44	1.52	2.30	0.70	8.83	15.96	19.01	0.19	0.11	100.07
4o	53.10	0.75	1.13	0.39	17.05	22.37	4.75	0.31	0.03	99.90
5c	51.49	1.48	2.20	0.59	10.87	15.53	17.66	0.17	0.12	100.11
5ac-o	52.96	0.90	1.00	0.32	19.65	21.59	3.59	0.33	0.04	100.39
7c-o	51.65	1.30	1.76	0.51	12.87	17.57	13.69	0.22	0.08	99.64
7c-o	52.89	0.83	0.84	0.24	19.65	21.66	3.16	0.35	0.02	99.64
Olivine	c=center	**Date**	11/14/92							
	e=edge									
Grain #	**SiO2**	**FeO**	**MgO**	**CaO**	**MnO**	**Total**				
Ac	36.21	30.51	31.91	0.07	0.27	98.97				
Ae	36.00	30.33	32.45	0.08	0.28	99.14				
Ee	35.74	33.87	29.36	0.12	0.32	99.42				

69

Table 22. (Continued) Microprobe data of 77017,161									
Pyroxene		Date	11/21/92						
		Time	16:27						
Grain #	SiO2	TiO2	Al2O3	Cr2O3	FeO	MgO	CaO	MnO	Na2O	Total
Fe	53.18	0.77	0.85	0.39	19.79	22.61	2.52	0.37	0.00	100.47
Gc	52.96	0.74	0.81	0.32	20.57	22.63	2.32	0.34	0.00	100.69
Ge	52.58	0.80	0.93	0.31	20.03	22.07	3.63	0.36	0.00	100.72
Hc	51.10	0.64	5.22	0.26	17.41	20.23	4.52	0.30	0.06	99.76
Ic	53.36	0.67	1.52	0.70	14.12	22.83	7.20	0.28	0.03	100.71

Table 23. Microprobe data of 78155,4										
Pyroxene		Date	11/7/92							
		Time	11:31							
Point #	SiO2	TiO2	Al2O3	Cr2O3	FeO	MgO	CaO	MnO	Na2O	Total
Λa	52.3384	0.957	1.4094	0.3876	16.5193	20.4406	8.7009	0.2666	0.0261	101.0459
Λb	51.7885	1.314	1.9347	0.5755	10.4372	16.4036	17.9489	0.2104	0.0666	100.6795

71

Table 24. Microprobe data of 78527,4										
Pyroxene		Date	11/6/92							
		Time	18:21							
Grain #	SiO2	TiO2	Al2O3	Cr2O3	FeO	MgO	CaO	MnO	Na2O	Total
2; 1a	52.89	1.52	1.58	0.61	5.48	16.72	20.83	0.12	0.24	99.98
2; 1b	54.83	1.13	1.18	0.55	10.40	24.49	7.98	0.18	0.06	100.82
Olivine		Date	11/14/92							
Grain #	SiO2	FeO	MgO	CaO	MnO	Total				
1; Ac	38.15	21.74	39.47	0.09	0.20	99.64				
1; Ae	38.08	21.60	39.49	0.07	0.20	99.44				
1; Bc	38.25	21.45	39.62	0.06	0.21	99.60				
1; Be	38.05	21.67	39.76	0.06	0.22	99.76				
Pyroxene	c=center	Date	11/18/92							
	e=edge	Time	8:00							
Grain #	SiO2	TiO2	Al2O3	Cr2O3	FeO	MgO	CaO	MnO	Na2O	Total
1;Cc1	55.48	0.76	0.96	0.51	13.14	27.82	1.77	0.21	0.01	100.66
1;Cc2	55.22	0.89	1.03	0.48	13.39	27.47	2.00	0.21	0.00	100.70

72

Table 25. Microprobe data of 79215,52						
Olivine	c=center c=edge	Date	11/14/92			
Grain #	SiO2	FeO	MgO	CaO	MnO	Total
4c	37.78	25.05	37.98	0.06	0.24	101.10
4c	37.86	24.82	37.95	0.13	0.25	101.01
1c	37.46	25.24	37.41	0.08	0.27	100.47
1e	37.44	25.58	37.33	0.08	0.25	100.68
5c	37.83	24.61	37.96	0.06	0.25	100.72
5e	37.79	24.63	38.21	0.11	0.27	101.01
7c	37.29	25.56	36.84	0.04	0.24	99.97
7e	37.74	26.14	37.06	0.06	0.26	101.25

73

Table 26. Microprobe data of 79125,71										
Pyroxene		Date	10/5/92							
		Time	14:00							
Grain #	SiO2	TiO2	Al2O3	Cr2O3	FeO	MgO	CaO	MnO	Na2O	Total
9a	52.43	1.58	2.11	0.54	6.61	16.40	20.20	0.14	0.12	100.12
9b	52.09	1.63	2.20	0.64	6.78	16.59	20.39	0.17	0.09	100.92
49	51.36	1.70	2.26	0.70	6.80	16.63	19.35	0.16	0.11	99.07
Pyroxene		Date	10/9/92							
Grain #	SiO2	TiO2	Al2O3	Cr2O3	FeO	MgO	CaO	MnO	Na2O	Total
18	51.41	1.72	2.45	0.71	6.51	16.64	20.67	0.13	0.15	100.38
23-2	51.71	1.73	2.35	0.61	6.35	16.78	20.79	0.13	0.13	100.59
54	51.95	1.78	2.45	0.58	6.58	16.57	20.59	0.14	0.15	100.79
28	54.25	0.70	1.10	0.37	14.46	28.16	1.37	0.26	0.02	100.68
72	52.17	1.72	2.48	0.65	6.18	16.40	20.94	0.13	0.14	100.81
83	52.00	1.66	2.32	0.56	6.63	16.62	20.84	0.17	0.15	100.94
85	54.14	0.87	1.29	0.41	14.34	27.53	1.79	0.23	0.01	100.61
96	52.48	1.58	2.11	0.57	6.72	16.82	19.99	0.14	0.14	100.55
95	54.82	0.73	1.03	0.38	14.51	27.56	1.68	0.28	0.01	101.00
97	51.81	1.82	2.43	0.62	6.50	16.42	20.68	0.14	0.15	100.56
Pyroxene		Date	5/2/93							
		Time	2:02							
Grain #	SiO2	TiO2	Al2O3	Cr2O3	FeO	MgO	CaO	MnO	Na2O	Total
1	51.86	1.78	2.26	0.67	6.66	16.66	20.30	0.21	0.11	100.51
2	51.95	1.77	2.21	0.57	6.98	16.86	19.78	0.18	0.12	100.42
3	51.85	1.82	2.33	0.67	6.87	16.77	19.71	0.16	0.12	100.29

APPENDIX C
SAMPLE DESCRIPTIONS

This appendix contains descriptions of the thin sections used in this study. It should be emphasized that since these samples are impact breccias, different thin sections of the same sample may display different textures. Sample locations were summarized by LSPET (1973), Ryder (1985), and Ryder and Norman (1980). Mineral compositions are listed in Appendix C.

Poikilitic I Samples
60035

The breccia consists of varying lithic clasts of mostly anorthositic troctolites(~60% plagioclase, ~20% opx, 15-20 olivine, and trace amounts of opaques/metals), with some norites (opx >> cpx), in a crushed, fine-grained matrix. The texture of the clasts is poikiloblastic, with pyroxene enclosing plagioclase and olivine grains, with a cataclastic overprint on the whole rock. Large (320-680 μm) plagioclase crystals also enclose small rounded olivines in a "necklace" formation near the crystal edges. Mafics grains in the clasts range from 20-150 μm in size. The oikocrysts are as large as 1.4 mm and plagioclase inclusions are between 40-140 μm in size.

67215

Most of this sample is matrix that consists of olivine noritic anorthosite (~80% plagioclase, ~18% mafics, and 1-2% opaques/metals). Two types of lithic clasts are present: gabbroic anorthosite (~70% plagioclase, ~15% mesostasis-clinopyroxene, ~10 % pyroxene grains, ~5% olivine, and minor amounts of metal

75

and spinels), and anorthosite (> 90% plagioclase, 3-5% pyroxene, and 2-5% mesostasis). The texture varies somewhat between clasts. Some clasts are sheared and others are poikilitic. The dominant pyroxene within the poikilitic clasts is clinopyroxene, which also exhibits exsolution lamellae and subgrains. A few clasts bear a more granular texture. The grain size in these metamorphosed clasts is variable. Some of the plagioclase grains are large (~0.8 mm) with jagged, scalloped edges and have shock features such as undulose extinction. The smaller (~120 μm) plagioclase grains are more polygonal, with rounded edges. The mafic grains range in size from 40-110 μm. Clast boundaries are well-integrated with the matrix. The matrix also varies in grain size and includes melt. The metamorphosed clasts are clustered together and are the most prominent type of clast.

67415

The clasts in this rock are mostly gabbroic anorthosites (~70% plagioclase, ~2% olivine, 25-30% pyroxene (cpx > opx), and ~2% ilmenite/chromite) with a few anorthosites (~97% plagioclase and ~3% opx). It is poikiloblastic in texture, with large opx grains enclosing subhedral plagioclase. Some, though not the majority, of the pyroxene oikocrysts have exsolution lamellae. The average grain sizes within the clasts are fairly large: pyroxene oikocrysts are ~0.7 mm, plagioclase inclusions are 340-600 μm, and the mafic inclusions are ~255 μm. The matrix grain sizes are 40-120 μm.

67955

The lithology of the clasts are olivine noritic anorthosites, with ~79% plagioclase, ~15% pyroxene, ~5% olivine, and ~1% opaques. As with 67915, 67955 has numerous lithic and mineral clasts. Much of the matrix consists of impact melt. The lithics also contain melt, with plagioclase, pyroxene, and

opaques (Fe-metal, ilmenite). The primary texture is poikilitic with a heavily cataclasized overprint, and some clasts have an igneous texture, with lathy plagioclase crystals. The olivine grains are also euhedral in morphology. As in the others, the oikocrysts and plagioclase grains are relatively large, ~1.2 mm and up to 880 μm, respectively. The mafic grain sizes range from 40-110 μm.

76230

The clasts are generally anorthositic olivine norites (50-60% plagioclase, 35-40% pyroxene, ~5% olivine, and ~2% ilmenite). The overall mineralogy consists of ~80% plagioclase, ~16% pyroxene, ~4% olivine, < 1% opaques, and mesostasis. Sample 76230 is poikilitic in texture, with large pyroxene oikocrysts enclosing euhedral to subrounded plagioclase crystals. A small number of the grains are subrounded and form triple junctions. The boundaries between the matrix and clasts are gradational, and some recrystallization is evident. The sizes for this thin section are: oikocrysts: 380 μm-0.98 mm; plagioclase: 60-270 μm, and the majority of the mafic grains are 20-30 μm, with some grains ~90 μm.

76235

This rock was taken off a boulder (part of an impact-melt breccia sheet) near the base of the North Massif in the Taurus-Littrow Valley (Warner et al., 1977). In thin section it is very similar to sample 76230, except the oikocrysts tend to be slightly larger (850 μm-1.2 mm). This particular thin section has a lithic clast (~1.25 mm) consisting of 4 plagioclase grains with a chain of olivine crystals forming a big ring (or necklace) around the entire lithic fragment. The plagioclase and mafic grain sizes are similar to those of 76230.

77017

Considered to be an extreme example of the poikilitic I group, this sample is the most 'igneous-looking' of the rocks in this study. Sample 77017 is

moderately ferroan in composition (Lindstrom and Lindstrom, 1986). The mineralogy of this gabbroic anorthosite is 65-70% plagioclase, 30-35% pyroxene (cpx > opx), ~5% olivine, and ~2% spinel. This rock consists of large pyroxene oikocrysts with blocky, euhedral plagioclase, resembling an orthocumulate texture. Large plagioclase grains enclose small, rounded olivine crystals. The grain size ranges from 130-280 μm. Shock veins also run through the sample.

Poikilitic II Samples

72559

Rock 72599 is a 27.85 g rake sample and was originally classified as a cataclastic anorthosite by Keil et al. (1974) upon examination of the hand sample. This olivine noritic anorthosite section contains ~75% plagioclase, ~25% mafics (opx and olivine), and trace amounts of spinel and metal. The poikilitic texture here is more pervasive than in 78527. There are very few lithic clasts, though there are a moderate number of large olivine fragments and plagioclase mineral fragments containing olivine "necklaces." A small area within this section has lathy plagioclase crystals. The grain size of rocks in this group is variable. The average grain size of the inclusions is ~7 μm, whereas the average mafic grain size in the matrix ranges from 35-50 μm.

73215

This sample is an olivine anorthositic norite (60-65% plagioclase, ~25% pyroxene, ~10% olivine, 2-3% spinel, and ~1% metal). Here the oikocrysts are predominantly orthopyroxene, with 2-3 smaller, rounder clinopyroxene oikocrysts within a thin section. The inclusions comprise subrounded to rounded plagioclase and olivine with an average diameter of 12 μm. Some of the inclusions have a granular texture. Grains outside of the oikocrysts are subhedral

78

to rounded, with a fairly granular texture (quadruple junctions). The average mafic grain size is ~40 μm. Some thin sections a greater range in grain size (10-80 μm) for the inclusions and the oikocrysts are more abundant, covering about 80% of the section.

78527

The modal mineralogy is 50-60% plagioclase, 45-50% orthopyroxene, and minor amounts of olivine, clinopyroxene, and spinel. The grains are more annealed and granular than those in the poikilitic I group, but this rock also contains small (< 1 mm) pyroxene (mostly low Ca) oikiocrysts, which are less pervasive than in the poikilitic I rocks. The matrix tends to coarsen towards plagioclase-rich areas. The boundaries between the matrix and clasts are not well-defined. There are some triple junctions, but many of the grains have jagged, scalloped edges. A few of the large plagioclase mineral fragments have olivine "necklace" inclusions. The pyroxene oikocrysts are subrounded and the inclusions consist of small, rounded plagioclase.

Granoblastic Samples
15418

Rock 15418 is a gabbroic anorthosite, consisting of 60-70% plagioclase, 20-30% pyroxene, 5-10% olivine, and ~3% opaques. The texture is granoblastic, with annealed grains as well as shock features. Many of the larger plagioclase grains (up to 0.5 cm) have a spongy texture, and most of the mafic grains are spherical. The mafic grains vary widely in size, from 25 to 130 μm.

67915

This section is rich in lithic and mineral clasts, with norites (~45% mafics (opx > cpx), ~40% plagioclase, ~3% spinel/ilmenite, and ~1% metal) and

troctolitic anorthosites comprising the main lithologies. The dominant texture of this sample is granoblastic. However, there are some areas with a poikilitic texture where small (~0.12 mm) plagioclase oikocrysts surround tiny, rounded pyroxenes and metal grains. Other plagioclase grains tend to have scalloped edges, are well annealed, and show undulose extinction. Rounded olivines (5-80 μm) are present and form triple junctions with plagioclase and pyroxene crystals. The boundaries between the clasts and matrix are gradational. Large (~0.6 mm), angular plagioclase fragments exist here as in many of the other samples, but without the olivine necklaces; this is characteristic of most granoblastic samples.

78155

The thin sections studied here have ~35% pyroxene, 5-7% olivine, 60-70% plagioclase, ~1% spinel, and minor traces of Fe-Ni metal and troilite. The matrix has an annealed texture with polygonal to irregularly shaped grains. The edges of the grains tend to be scalloped and/or corrugated. Many of the plagioclase mineral fragments (maximum size of 0.5 mm) have small, rounded olivines scattered throughout them as well as in necklace formation. The boundaries between the clasts and matrix are indistinct. The clasts are a more mafic version of the matrix. Some may contain yet another clast. The average mafic grain size in the matrix is ~25 μm.

79215

Sample 79215 is an olivine noritic anorthosite consisting of ~65% plagioclase, ~5% olivine, ~20% pyroxene, and minor amounts of apatite, chromite, ilmenite, troilite, and Fe-Ni-Co metal. The texture is very fine-grained (~ 20 μm) and granoblastic with numerous triple junctions. The transition from matrix to clast is gradational, and the grain size varied only slightly from region

to region. There was only one plagioclase mineral fragment with scalloped edges and an olivine necklace (at the edge of the plagioclase grain).

APPENDIX D
IMAGE PROCESSING CORRECTIONS

NIH Image, version 1.44, was used to obtain grain size measurements of sample 79215,52. The table below lists the actual and measured circumferences of circles used to obtain correction factors for grain sizes measured using Analyze Particles under the Analyze menu of the program. Ludwig (1993) has investigated the correction factors necessary when analyzing fractures and triangular shaped areas.

Table 27. CSD Correction Factors for Image 1.44

Circle	Actual Diam. (μm)	Actual Circum. (μm)	Analyze Particles Circum. (μm)	Correction Factor (AP/Actual)
3	903.00	2836.86	3005.80	1.060
4	491.43	1543.87	1647.38	1.067
1	165.86	521.07	561.00	1.077
2	76.78	241.21	276.68	1.147
5	24.57	77.19	94.07	1.218
6	18.43	57.90	69.50	1.200

REFERENCES

Ashwal, L.D. Petrologic Evidence for a Plutonic Igneous Origin of Anorthositic Norite Clasts in 67955 and 77017. *Proc. Lunar Sci. Conf. 6th*, 221-230, 1975.

Bickel, C.E., Warner, J.L., and Phinney, W.C. Petrology of 79215: Brecciation of a Lunar Cumulate. *Proc. Lunar Sci. Conf. 7th*, 1793-1819, 1976.

Bickel, C.E. Petrology of 78155: An Early, Thermally Metamorphosed Polymict Breccia. *Proc. Lunar Sci. Conf. 8th*, 2007-2027, 1977.

Bickel, C.E. and Warner, J.L. Survey of Lunar Plutonic and Granulitic Lithic Fragments. *Proc. Lunar Planet. Sci. Conf. 9th*, 629-652, 1978.

Blanchard, D.P., Jacobs, J.W., and Brannon, J.C. Chemistry of ANT-suite and Felsite Clasts from Consortium Breccia 73215 and of Gabbroic Anorthosite 79215. *Proc. Lunar Sci. Conf. 8th*, 2507-2524, 1977.

Cadogan, P.H. and Turner, G. The Chronology of the Apollo 17 Station 6 Boulder. *Proc. Lunar Sci. Conf. 7th*, 2267-2285, 1976.

Cashman, K.V and Ferry, J.M. Crystal Size Distribution (CSD) in Rocks and the Kinetics and Dynamics of Crystallization, III. Metamorphic Crystallization. *Contrib. Miner. Petr.*, **99**, 401-415, 1988.

Cashman, K.V and Marsh, B.D. Crystal Size Distribution (CSD) in Rocks and the Kinetics and Dynamics of Crystallization, II. Makaopuhi Lava Lake. *Contrib. Miner. Petr.*, **99**, 292-305, 1988.

Christie, J.M., Griggs, D.T., Heuer, A.H., Nord, G.L., Radcliffe, S.V., Lally, J.S., and Fisher, R.M. Electron Petrography of Apollo 14 and 15 Breccias and Shock-produced Analogs. *Proc. Lunar Sci. Conf. 4th*, 365-382, 1973.

Cushing, J.A., Taylor, G.J, Norman, M.D., and Keil, K. Refining the Granulite Suite (abstract). *Workshop on Geology of Apollo 17 Landing Site* (G. Ryder, H.H. Schmitt, and P.D. Spudis, eds.), LPI Tech Rpt. 92- 09, Part 1, Houston: LPI 1992.

Dence, M.R., Grieve, R.A.F., and Plant, A.G. Apollo 17 Grey Breccias and Crustal Composition in the Serenitatis Basin Region. *Proc. Lunar Sci. Conf. 7th*, 1821-1832, 1976.

Doherty, R.D. Diffusive Phase Transformations in the Solid State. In *Physical Metallurgy* (Cahn, R.W. and Haasen, P., eds.). Amsterdam: North-Holland Physics Publishing, 933-1030, 1983.

Ebihara, M., Wolf, R., Warren, P.H., and Anders, E. Trace Elements in 59 Mostly Highland Moon Rocks. *Proc. Lunar Planet. Sci. Conf. 22nd*, 417-426, 1992.

Fischmeister, H. and Grimvall, G. Ostwald Ripening—A Survey. In *Sintering and Related Phenomena* (Kuczynski, G.C., ed.), *Mat. Sci. Res.*, **6** , 119-149, 1973.

Frost, B.R. and Lindsley, D.H. Equilibria Among Fe-Ti Oxides, Pyroxenes, Olivine, and Quartz: Part II. Application. *Amer. Mineral.*, **77**, 1004-1020, 1992.

Gray, N., and Kirkpatrick, R.J. Nucleation and Growth of Plagioclase, Makaopuhi and Alae Lava Lakes, Kilauea Volcano, Hawaii: Discussion and Reply. *GSA Bull.*, **89**, 797-800, 1978.

Greenwood, G.W. Particle Coarsening. In *The Mechanism of Phase Transformations in Crystalline Solids*, Regent Series #33. London: Institute of Metals, 1969.

Grieve, R.A.F., McKay, G.A., Smith, H.D., and Weill, D.F. Lunar Polymict Breccia 14321: A Petrographic Study. *Geochim. Cosmochim. Acta*, **39**, 229-246, 1975.

Grieve, R.A.F. Cratering in the Lunar Highlands: Some Problems with the Process, Record, and Effects. In *Proc. Conf. Lunar Highlands Crust* (Papike, J.J. and Merrill, R.B., eds.), 173-196, 1980.

Hodges, F.N. and Kushiro, I. Apollo 17 Petrology and Experimental Determination of Differentiation Sequences in Model Moon Compositions. *Proc. Lunar Sci. Conf. 5th,* 505-520, 1974.

Hollister, L.S. Sample 67955: A Description and a Problem. *Proc. Lunar Sci. Conf. 4th,* 633-641, 1973.

Hörz, F., Gibbons, R.V., Hill, R.E., and Gault, D.E. Large Scale Cratering of the Lunar Highlands: Some Monte Carlo Model Considerations. *Proc. Lunar Sci. Conf. 7th,* 2931-2945, 1976.

Hubbard, N.J., Rhodes, J.M., Wiesmann, H., Shih, C.Y., and Bansal, B.M. The Chemical Definition and Interpretation of Rock Types Returned from the Non-mare Regions of the Moon. *Proc. Lunar Sci. Conf. 5th,* 1227-1246, 1974.

Jaeger, J.C. Cooling and Solidification of Igneous Rocks, in Basalts, **2** (Hess, H.H. and Poldervaart, A., eds.). Sydney: John Wiley & Sons, 503-536, 1968 .

James, O.B. and Hammarstrom, J.G. Petrology of Four Clasts from Consortium Breccia 73215. *Proc. Lunar Sci. Conf. 8th,* 2459-2494, 1977.

James, O.B. Rocks of the Early Lunar Crust. *Proc. Lunar Planet. Sci. Conf. 11th,* 365-393, 1980.

Jones, K.A., and Galwey, A.K. Size Distribution, Composition and Growth Kinetics of Garnet Crystals of Some Metamorphic Rocks from West of Ireland. *Quart. Jl. Geol. Soc. London,* **122**, 29-44, 1966.

Jones, R.H. and Rubie, D.C. Thermal Histories of CO3 Chondrites: Application of Olivine Diffusion Modelling to Parent Body Metamorphism. *Earth Planet. Sci. Lett.,* **106**, 73-86, 1991.

Jurewicz, S.R. and Watson, E.B. The Distribution of Partial Melt in a Granitic System: The Application of Liquid Phase Sintering Theory. *Geochim. Cosmochim. Acta,* **49**, 1109-1121, 1985.

Juster, T., Defant, M.J., and Jones, H. Stereological Effects on Crystal Size Distributions of Orthorhombic and Tetragonal Crystals. Submitted to *Contrib. Miner. Petrol.*, 1992.

Keil, K., Dowty, E., and Prinz, M. Description, Classification and Inventory of 113 Apollo 17 Rake Samples from Stations 1A, 2, 7, and 8. NASA, Johnson Space Center, Houston, 149 pp., 1974.

Kirkpatrick, R.J. Nucleation and Growth of Plagioclase, Makaopuhi and Alae Lava Lakes, Kilauea Volcano, Hawaii. *GSA Bull.*, **88**, 78-84, 1977.

Kirsten, T. and Horn, P. Chronology of the Taurus-Littrow Region III: Ages of Mare Basalts and Highland Breccias and Some Remarks about the Interpretation of Lunar Highland Rock Ages. *Proc. Lunar Sci. Conf. 5th*, 1451-1475, 1974.

Kretz, R. Grain-size Distribution for Certain Metamorphic Minerals in Relation to Nucleation and Growth. *J. Geol.*, **74**, 147-173, 1966.

Kretz, R. Transfer and Exchange Equilibria in a Portion of the Pyroxene Quadrilateral as Deduced from Natural and Experimental Data. *Geochim. Cosmochim. Acta*, **46**, 411-421, 1982.

Laul, J.C., Hill, D.W., and Schmitt, R.A. Chemical Studies of Apollo 16 and 17 Samples. *Proc. Lunar Sci. Conf. 5th*, 1047-1066, 1974.

Lindsley, D.H. and Frost, B.R. Equilibria Among Fe-Ti Oxides, Pyroxenes, Olivine, and Quartz: Part I. Theory. *Amer. Mineral.*, **77**, 987-1003, 1992.

Lindstrom, M.M., Nava, D.F., Lindstrom, D.J., Winzer, S.R., Lum, R.K.L., Schuhmann, P.J., Schuhmann, S., and Philpotts, J.A. Geochemical Studies of the White Breccia Boulders at North Ray Crater, Descartes Region of the Lunar Highlands. *Proc. Lunar Sci. Conf. 8th*, 2137-2151, 1977.

Lindstrom, M.M. and Salpas, P.A. Geochemical Studies of Rocks from North Ray Crater, Apollo 16. *Proc. Lunar Planet. Sci. Conf. 12th*, 305-322, 1981.

Lindstrom, M.M. and Salpas, P.A. Geochemical Studies of Feldspathic Fragmental Breccias and the Nature of North Ray Crater Ejecta. *Proc. Lunar Planet. Sci. Conf. 13th, in J. Geophy. Res. Supplem.*, **88**, A671-A683, 1983.

Lindstrom, M.M. and Lindstrom, D.J. Lunar Granulites and Their Precursor Anorthositic Norites of the Early Lunar Crust. *Proc. Lunar Planet. Sci. Conf. 16th,* in *J. Geoph. Res. Supplem.*, **91** (B4), D263-D276, 1986.

LSPET (Lunar Sample Preliminary Examination Team). Apollo 17 Lunar Samples: Chemical and Petrographic Description. *Science*, **182**, 659-671, 1973.

Ludwig, N.A. The Geometry, Distribution and Orientation of Pore Space in Oceanic Crust Extrusives: Constraints from the Troodos Ophiolite, Cyprus. M.S. thesis, Univ. of Hawaii, Honolulu, HI., 1993.

Markworth, A.J., The Kinetic Behavior of Precipitate Particles Under Ostwald Ripening Conditions. *Metallography*, **3**, 197-208, 1970.

Marsh, B.D. Crystal Size Distribution (CSD) in Rocks and the Kinetics and Dynamics of Crystallization, I. Theory. *Contrib. Miner. Petr.*, **99**, 277-291, 1988.

Marti, K., Aeschlimann, U., Eberhardt, P., Geiss, J., Grögler, N., Jost, D.T., Laul, J.C., Ma, M.S., Schmitt, R.A., and Taylor, G.J. Pieces of the Ancient Lunar Crust: Ages and Composition of Clasts in Consortium Breccia 67915. *Proc. Lunar Planet. Sci. Conf. 14th, in J. Geoph. Res. Supplem.*, **88**, B165-B175, 1983.

Martin, J.W. and Doherty, R.D. Stability of Microstructure in Metallic Systems. Cambridge: Cambridge University Press, 298 pp., 1976.

McCallum, I.S., Mathez, E.A., Okamura, F.P., and Ghose, S. Petrology and Crystal Chemistry of Poikilitic Anorthositic Gabbro 77017. *Proc. Lunar Sci. Conf. 5th,* 287-302, 1974.

McCoy, T.J. Metamorphism, Brecciation and Parent Body Structures of LL-group Chondrites. M.S. thesis, Univ. of New Mexico, 1990.

McCoy, T.J., Scott, E.R., Jones, R.H., Keil, K., and Taylor, G.J. Composition of
Chondrule Silicates in LL3-5 Chondrites and Implications for Their Nebular
History and Parent Body Metamorphism.. *Geochim. Cosmochim. Acta*, **55**, 601-
619, 1991.

McGee, J.J., Bence, A.E., Eichhorn, G., and Schaeffer, O.A. Feldspathic Granulite
79215: Limitations on T-f_{O_2} Conditions and Time of Metamorphism. *Proc.
Lunar Planet. Sci. Conf. 9th*, 743-772, 1978.

McGee, J.J. Petrology of Brecciated Ferroan Noritic Anorthosite 67215. *Proc. Lunar
Planet. Sci. Conf. 18th*, 21-31, 1988.

Miller, D.S. and Wagner, G.A. Age and Intensity of Thermal Events by Fission Track
Analysis: The Ries Impact Crater. *Earth Planet. Sci. Lett.*, **43**, 351-358, 1979.

Misener, D.J. Cationic Diffusion in Olivine to 1400C and 35 kbar. Geochimal
Transport and Kinetics, Publ. 634, Carnegie Institue, Washington, D.C., 117-
129, 1974.

Morgan, J.W., Gros, J., Takahashi, H., and Hertogen, J. Lunar Breccia 73215:
Siderophile and Volatile Trace Elements. *Proc. Lunar Sci. Conf. 7th* , 2189-
2199,   1976.

Morgan, J.W. and Petrie, R.K. Breccias 73215 and 73255: Siderophile and Volatile
Trace Elements. *Proc. Lunar Planet. Sci. Conf. 10th*, 789-801, 1979.

Nehru, C.E., Warner, R.D., Keil, K., and Taylor, G.J. Metamorphism of Brecciated
ANT Rocks: Anorthositic Troctolite 72559 and Norite 78527. *Proc. Lunar
Planet. Sci. Conf. 9th*, 773-788, 1978.

Nord, G.L., Christie, J.M., Heuer, A.H., and Lally, J.S. North Ray Crater Breccias: An
Electron Petrographic Study. *Proc. Lunar Sci. Conf. 6th*, 779-797, 1975.

Nunes, P.D., Tatsumoto, M., and Unruh, D.M. U-Th-Pb Systematics of Anorthositic Gabbros 78155 and 77017—Implications for Early Lunar Evolution. *Proc. Lunar Sci. Conf. 6th*, 1431-1444, 1975. ·

Richter, D., Simmons, G., and Siegfried, R. Microcracks, Micropores, and Their Petrologic Interpretation for 72415 and 15418. *Proc. Lunar Sci. Conf. 7th*, 1901-1923, 1976.

Rose, H.J., Baedecker, P.A., Berman, S., Christian, R.P., Dwornik, E.J., Finkelman, R.B., and Schnepfe, M.M. Chemical Composition of Rocks and Soils Returned by the Apollo 15, 16, and 17 Missions. *Proc. Lunar Sci. Conf. 6th*, 1363-1373, 1975.

Ryder, G. and Norman, M.D. Catalog of Apollo 16 Rocks, vol. 1-3. *JSC Publication 16904*, 1144 pp., 1980.

Ryder, G. Catalog of Apollo 15 Rocks, vol. 1-3. *JSC Publication 20787*, 1985.

Shaw, N.J. Densification and Coarsening During Solid State Sintering of Ceramics: A Review of the Models. II. Grain Growth. *Advanced Ceramics, PMI.*, **21** (5), 31-33, 1989.

Smith, J.V., Hansen, E.C., and Steele, I.M. Lunar Highland Rocks: Element Partitioning Among Minerals II: Electron Microprobe Analyses of Al, P, Ca, Ti, Cr, Mn, and Fe in Olivine. *Proc. Lunar Planet. Sci. Conf. 11th*, 555-569, 1980.

Steele, I.M., Hutcheon, I.D., and Smith, J.V. Ion Microprobe Analysis and Petrogenetic Interpretations of Li, Mg, Ti, K, Sr, Ba in Lunar Plagioclase. *Proc. Lunar Planet. Sci. Conf. 11th*, 571-590, 1980.

Stettler, A.., Eberhardt, P., Geiss, J., Grögler, N., and Maurer, P. Ar^{39}-Ar^{40} Ages and Ar^{37}-Ar^{38} Exposure Ages of Lunar Rocks. *Lunar Sci. Conf. 4th*, 1865-1888, 1973.

Stewart, D.B. Apollonian Metamorphic Rocks—the Products of Prolonged Subsolidus Equilibration (abstract). *Lunar Sci. Conf. VI*, 774-776, 1975.

Stöffler, D. Cratering Mechanics: Data from Terrestrial and Experimental Craters and Implications for the Apollo 16 Site (abstract). In *Workshop on Apollo 16* (O.B. James, ed.), LPI Tech Rpt. 81-01, 132-141, 1981.

Stöffler, D., Bischoff, A.., Borchardt, R., Burghele, A., Deutsch, A., Jessberger, E.K., Osertag, R., Palme, H., Spettel, B., Reimold, W.U., Wacher, K., and Wänke, H. Composition and Evolution of the Lunar Crust in the Descartes Highlands, Apollo 16. *Proc. Lunar Planet. Sci. Conf. 15th, in J. Geophy. Res. Supplem.*, **90**, C449-C506, 1985.

Taylor, G.J. and Mosie, A.B. Breccia Guidebook No. 3: 67915. *JSC Publication 16242*, 43 pp., 1979.

Taylor, G.J., Warren, P., Ryder, G., Delano, J., Pieters, C., and Lofgren, G. Lunar Rocks. In *Lunar Sourcebook* (Heiken, G., Vaniman, D., and French, B.M., eds.). New York: Cambridge University Press, 736 pp., 1991.

Taylor, S.R., Lunar Science: A Post-Apollo View. New York: Pergamon, pp. 372, 1975.

Taylor, S.R. Planetary Science: A Lunar Perspective. Houston: Lunar and Planetary Inst., pp. 481, 1982.

Turner, G. and Cadogan, P.H. The History of Lunar Bombardment Inferred from [40]Ar-[39]Ar Dating of Highland Rocks. *Proc. Lunar Sci. Conf. 6th*, 1509-1538, 1975.

Uhlmann, D.R., Yinnon, H., and Fang, C.-Y. Simplified Model Evaluation of Cooling Rates for Glass-containing Lunar Compositions. *Proc. Lunar Planet. Sci. Conf. 12th*, 281-288, 1981.

Vander Voort, G.F. Metallography: Principles and Practice. San Francisco: McGraw-Hill Book Co., 752 pp., 1984.

Wänke, H., Palme, H., Kruse, H., Baddenhausen, H., Cendales, M., Dreibus, G., Hofmeister, H., Jagoutz, E., Palme, C., Spettel, B., and Thacker, R. Chemistry of Lunar Highland Rocks: A Refined Evaluation of the Composition of the Primary Matter. *Proc. Lunar Sci. Conf. 7th*, 3479-3499, 1976.

Warner, J.L., Phinney, W.C., Bickel, C.E., and Simonds, C.H. Feldspathic Granulitic Impactites and Pre-final Bombardment Lunar Evolution. *Proc. Lunar Sci. Conf. 8th*, 2051-2066, 1977.

Warner, R.D., Taylor, G.J., and Keil, K. Petrology of 60035: Evolution of a Polymict ANT Breccia. *Proc. Conf. Lunar Highlands Crust*, 377-394, 1980.

Warren, P.H. and Wasson, J.T. Pristine Nonmare Rocks and the Nature of the Lunar Crust. *Proc. Lunar Sci. Conf. 8th,* 2215-2235, 1977.

Weiblen, P.W., Day, W.C., and Miller, J.D. Significance of Major and Minor Element Variations in Plagioclase in Sodic Ferrogabbro and Breccia Matrix in Lunar Highlands Sample 67915. *Proc. Lunar Planet. Sci. Conf. 11th*, 591-610, 1980.